Official Journal of CIOMP
elight.springeropen.com

REVIEW

Open Access

Hot-electron dynamics in plasmonic nanostructures: fundamentals, applications and overlooked aspects

Jacob Khurgin[1], Anton Yu. Bykov[2] and Anatoly V. Zayats[2*]

Abstract

Light absorption near a surface of conductive materials and nanostructures leads to the excitation of nonequilibrium, high-energy charge carriers: electrons above the Fermi level or holes below it. When remaining inside a material, these so-called hot carriers result in nonlinear, Kerr-type, optical effects important for controlling light with light. They can also transfer into the surroundings of the nanostructures, resulting in photocurrent, or they can interact with adjacent molecules and media, inducing photochemical transformations. Understanding the dynamics of hot carriers and related effects in plasmonic nanostructures is important for the development of ultrafast detectors and nonlinear optical components, broadband photocatalysis, enhanced nanoscale optoelectronic devices, nanoscale and ultrafast temperature control, and other technologies of tomorrow. In this review, we will discuss the fundamentals of plasmonically-engendered hot electrons, focusing on the overlooked aspects, theoretical descriptions and experimental methods to study them, and describe prototypical processes and examples of most promising applications of hot-electron processes at the metal interfaces.

Nonequilibrium charge carriers are important in many fields of physics and chemistry and explored in metallic and semiconducting materials to control nonlinear optical response, photodetection, electronic tunnelling and chemical reactions to name but a few [1–5]. Upon absorption of light in material, electrons and/or holes with excess energy (hot carriers) can be created. The excess energy depends on a photon energy as well as a material band structure. In semiconductors, the photon energy should exceed a band gap, while in metals (or doped semiconductors), photon absorption can take place through both interband and intraband—within the conduction band—transitions. The latter is facilitated by plasmonic excitations.

The field of plasmonics has experienced steady progress, through the development of our understanding of the optical properties of complex nanoscale metal structures to their application in sensing, information processing and nanomedicine [6–8]. Most of these applications are based simply on the strong field localization and high field enhancement near a metal surface, found in plasmonic nanostructures. However, the phenomena associated with the effect of the high fields on behaviour of electrons within the metal nanostructures have been largely ignored until recently. These effects arise from the same coherent oscillations of free electrons (surface plasmons) and are capable of significantly influencing physical and chemical processes near the metal surface, not only because of the high electric fields but also as a result of the changing electron energy distribution and/or transfer of energetic electrons from the metal to adjacent molecules or materials in the surroundings.

*Correspondence:
Anatoly V. Zayats
anatoly.zayats@kcl.ac.uk
[1] Electrical and Computer Engineering Department, Johns Hopkins University, Baltimore, MD, USA
[2] Department of Physics and London Centre for Nanotechnology, King's College London, Strand, London WC2R 2LS, UK

Plasmonic excitations are interchangeably referred to as surface plasmons or surface plasmon polaritons (SPPs) on smooth metal interfaces or localized surface plasmons (LSPs) [6] on nanostructures and nanoparticles. Strictly speaking the term "plasmon" defines oscillations of charge density in free-electron plasma, while the term "plasmon polariton" describes a quasiparticle in which a plasmon is coupled with a photon of electromagnetic field. It is the electric component of this field that is responsible for the interaction between plasmon polaritons and individual free carriers in the Fermi sea of electrons that leads to strong light absorption and efficient hot-carrier generation.

Generation of hot electrons in plasmonic structures via surface plasmon excitations has several important advantages: (1) high generation efficiency related to strong light absorption via plasmonic resonances; (2) broad energy spectrum of the hot-electrons related to the broadband nature of plasmonic excitations (not limited by semiconductor bandgaps, the hot-electron energy can be tuned simply by changing the excitation wavelength); (3) high density of hot electrons in a spatially well-defined volume near a plasmonic metal surface, from where they can be efficiently extracted before they thermalise in the metal by engineering resonant charge transfer to proximal molecules or semiconductors.

Initial carrier distribution is non-thermal and evolves in complex ways through internal thermalisation as well as external processes, such as carrier or energy transfer into surrounding environment, influencing variety of processes. The hot-carrier relaxation time is determined by the interplay between electron–electron, electron–phonon scattering and carrier extraction probabilities and can be controlled by engineering the nanostructure shape and pathways of interaction with surrounding environment.

In thermal equilibrium, the energy distribution of the electrons is determined by a temperature which is the same as a lattice temperature. Nonequilibrium hot carriers have an energy distribution which cannot be assigned a single temperature (nonthermal distribution). Thermalisation process results in the thermal Fermi–Dirac distribution of the hot carriers which is characterized by a temperature distinct from a lattice temperature, and, in turn, the lattice (phonon) temperature can differ from the temperature of surroundings. Thermal hot carriers, which are on average much less energetic than non-thermal ones, will then further loose the energy to phonons, heating the lattice. These hot-electron thermalisation processes take place on different time scales and hot electrons with different energies are important in context of diverse physical and chemical processes.

In this Review, we discuss microscopic picture of the hot-electron generation and evolution in plasmonic nanostructures and related macroscopic effects, including control of nonequilibrium electrons in nanostructures as well as plasmonic nanostructures as a source of hot electrons in semiconductors and molecules. We start with description of the light absorption in plasmonic nanoparticles, introduce the relevant thermalisation processes and discuss hot-carrier generation rate. Both continuous wave (CW), such as solar, and pulsed, such as femtosecond laser, excitations are considered and contrasted. After the comparison of the hot carrier generation mechanisms, the injection of hot-electrons across the metal interface is discussed, in particular at the metal–semiconductor interfaces. The chemical effects related to hot-carrier interactions with surroundings are also considered and their influence on hot-carrier dynamics. Finally, nonlinear optical response induced in plasmonic nanostructures by hot-carrier excitation is discussed, and their role as a tool for understanding hot-electron processes.

1 Hot-electron generation and relaxation

1.1 Discrete (quantum) nature of hot carrier generation and decay

To better understand the importance of quantum character of the processes that take place when hot carriers are generated and decay, from the very start we shall point to the difference between pulsed laser illumination which can achieve power densities on GW cm^{-2} scales and the illumination with thermal or other incoherent light sources limited to 100s of W cm^{-2} irradiance (e.g., 100 W cm^{-2} is roughly 1000 times that of the irradiance of the Sun at the equator). It is the latter, CW excitation case with low to moderate intensities that is beneficial for practical applications in solar-driven chemistry, while the former is important for high value chemical synthesis as well as serves as a tool for the study and understanding of carrier dynamics on the femtosecond scale and applications in nonlinear optics.

Let us consider an ensemble of identical plasmonic spherical nanoparticles of diameter d = 5–30 nm illuminated with light at the wavelength corresponding to the LSP resonance (Fig. 1a). Under CW irradiation (e.g., $I_{in} = 100\ \mathrm{W\ cm^{-2}}$), fraction of nanoparticles excited at any given time can be estimated by noting that the electric field in the LSP mode gets enhanced approximately by a factor of $Q = \omega/\gamma$, where γ is the total (radiative and nonradiative) decay rate of

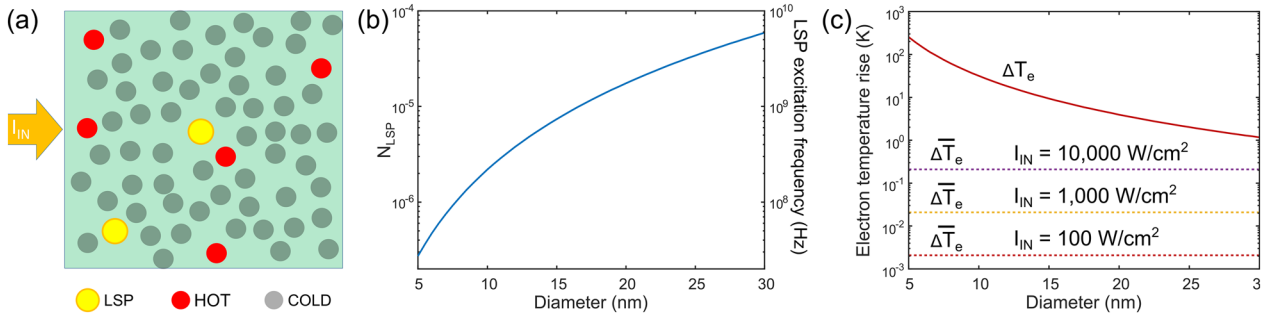

Fig. 1 Discrete character of hot-carrier excitation in nanoparticles and its implications. **a** Excitation and decay of LSPs and nonequilibrium carriers in the nanosphere ensemble illuminated by a CW light with irradiance I_{in} at a given moment in time: LSPs (orange rings) are excited on a few nanoparticles (yellow), nonequilibrium hot carriers are excited in a few "hot" nanoparticles (red), while the electrons in the vast majority of nanoparticles remain "cold", i.e. close to the lattice temperature T_L (although T_L may itself be significantly elevated relative to the ambient temperature). **b** Probability of a LSP being excited on a given nanoparticle at a given moment in time, N_{LSP}, and the frequency of excitation, f_{LSP}, for the irradiance $I_{in} = 100$ W cm^{-2}. **c** Instant rise of the electron temperature, ΔT_e, following the decay of the LSP (solid line), which is independent of I_{in}, and the rise of the time-averaged electron temperature, $\Delta\overline{T_e}$, relative to the lattice temperature (dashed lines) if one neglects the quantum nature of the absorption process, for three different values of I_{in}

the LSP mode at the frequency ω [9, 10]. This factor is $Q \sim 10-20$ for good plasmonic metals, such as Au or Ag [11], and even less than that for small nanoparticles where the Landau damping is prevalent [12]. Therefore, the energy density in the LSP mode can be found approximately as $Q^2 I_{in}/c$, where c is the speed of light, and the total energy residing on a given nanoparticle at a given time is $U_{LSP} \sim Q^2(I_{in}/c)V_{eff}$, where V_{eff} is the effective volume of the LSP mode that is commensurate with the volume V of the nanoparticle itself. The number of LSPs per one nanoparticle (which is the same as the fraction of all nanoparticles that has an LSP residing on it at a given time) is, therefore, $N_{LSP} \sim Q^2(I_{in}/c)V_{eff}/\hbar\omega$. For the illuminating light with $\hbar\omega = 2$ eV and $Q = 20$ (corresponding to $\gamma \sim 1.5 \times 10^{14} s^{-1}$), this gives $N_{LSP} << 1$, ranging from 2×10^{-7} to 6×10^{-5} depending on the nanoparticle size (Fig. 1b). This means that, for example, for a nanoparticle with a diameter of 20 nm and CW illumination, at a given time only 0.002% of the nanoparticles actually have an LSP on them while the vast majority do not have any. This situation is depicted in Fig. 1a where only a few nanoparticles are excited at a given time, i.e. have an LSP on them (shown in yellow) or carry hot carriers generated as a result of the LSP decay (shown in red), while most of the nanoparticles remain "cold", meaning that either they were not excited yet or the hot carriers that had been previously excited in them have already thermalized and transferred their energy to the lattice.

In more sophisticated plasmonic arrangements involving various nanoantenna or nanofocusing geometries, the total field enhancement does not exceed Q^2 [13–16]. It is easy to see that even for nanoparticles as large as 50 nm, the condition $N_{LSP} << 1$ is still maintained. It would take $I_{in} > 5$ MW cm^{-2} to achieve situation where each nanoparticle has on average more than a single LSP—this situation can of course occur for pulsed laser excitation [17–20].

Even if the concentration of the nanoparticles is high enough to achieve very strong (even total) absorption of the incident light, one can easily estimate the frequency with which the LSPs are generated on a given nanoparticle as simply $f_{LSP} = \gamma N_{LSP} = Q(I_{in}/\hbar c)V_{eff}$ (Fig. 1b). For the aforementioned case of d = 20 nm, $f_{LSP} \sim 2.5$ GHz. Therefore, the LSP on an individual nanoparticle is excited approximately every 400 ps and then decays within brief time $\tau_{LSP} \sim \gamma^{-1} \sim 7$ fs [17, 19, 21, 22]. Since the radiative decay rate of the LSP is on the order of $\gamma_{rad} \sim \omega V_{eff}/\lambda^3 \sim 10^{11}$ s^{-1} [23], it can be neglected and γ can be considered to be almost entirely nonradiative, i.e. each time LSP decays, an electron–hole pair gets generated in the metal.

The generated electron–hole pair in turn survives for a very short time, as it is subject to both electron–electron (EE) and electron–phonon (EP) scattering processes with scattering rates γ_{ee} and γ_{ep}, respectively [24]. While these rates in noble metals are similar (of the order 10^{13}–10^{14} s^{-1}) [25], the actual rate of energy transfer to the lattice, γ_{EL}, is significantly lower than that because the energy of a typical phonon (i.e., the Debye energy) is many times smaller than the LSP energy $\hbar\omega$. It takes, therefore, many EP scattering events to transfer all the energy from the carriers to the lattice and to subsequently raise its temperature by $\Delta T_L = \hbar\omega/c_L NV$ per each decayed LSP, where c_L is the molar specific heat of the lattice and N is the number of atoms per unit volume (for metals with a single valence electron which is free, such as gold or silver, N is equal to the electron concentration $N_e \sim 6 \times 10^{22}$ cm^{-3}) [26]. At the same time, since

in each EE scattering event the energy of a hot carrier is shared between three carriers (the original electron (hole) is scattered and a new electron–hole pair is created when the electron is promoted from below to above the Fermi level), it takes only a very few of those events to spread the initial LSP energy $\hbar\omega$ between all the electrons near the Fermi level and raise the electron temperature by $\Delta T_e = \hbar\omega/c_e N_e V$, where $c_e << c_L$ is the specific heat of the electrons [24]. Therefore, one can introduce the electron thermalization time τ_E, which is only a few times longer than the EE scattering time $\tau_{ee} = \gamma_{ee}^{-1}$ and is many times shorter than the electron cooling rate $\tau_{EL} = \gamma_{EL}^{-1}$, which in turn is at least an order of magnitude longer than the EP scattering time $\tau_{ep} = \gamma_{ep}^{-1}$.

Let us now consider the dynamics of the processes occurring in a given nanoparticle (the labels in the list below correspond to the panels in Fig. 2):

(a) First, at time t_0, a LSP is generated in the "cold" nanoparticle (Fig. 2a), where the electrons are in equilibrium with the lattice and have the temperature $T_e = T_{L0}$ to which lattice temperature decays between the excitations. This temperature corresponds to the ambient temperature T_0 only before the illuminating light is turned on is not much different from the time-average lattice temperature $\overline{T}_L$ after several excitation cycles (the variation of the average lattice temperature with time is not shown in Fig. 2f as it depends on various factors as discussed below).

(b) Then, at time $t_1 \sim t_0 + \tau_{LSP}$, LSP decays engendering a single "primary" or "first generation" electron–hole pair, creating a non-thermal carrier distribution which cannot be assigned an electron temperature.

(c) Roughly at time $t_2 \sim t_1 + \tau_{ee}$, each of the primary carriers undergoes a collision with the electron below the Fermi level and its energy is shared between three second generation carriers—two electrons and one hole (or two holes and one electron). The second-generation carriers follow the same routine and, with only a few generations at time $t_3 \sim t_2 + \tau_E$, a thermal quasi-equilibrium is reached. The term "quasi" is used here to indicate that the carrier distribution strictly cannot be described by a simple Fermi–Dirac function with a well-defined single temperature T_e [27, 28]. For a simple analysis, we can estimate the electron temperature rise using the electron specific heat $c_e = \pi^2 k_B^2 T_e/2E_F$, where E_F is the Fermi energy

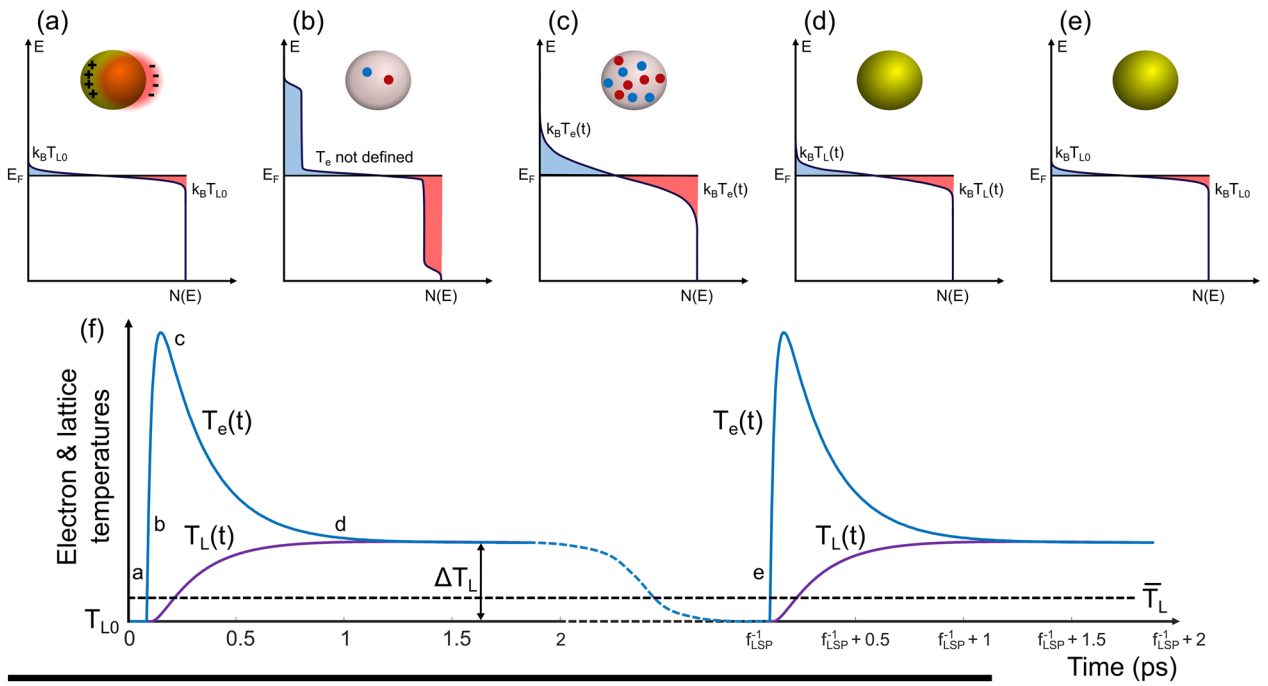

Fig. 2 Evolution of hot carriers in a plasmonic nanoparticle. **a**–**e** Energy distribution of electrons in a nanoparticle at different times **a** before and **b** immediately after the LSP decay, **c** after thermalization of carriers and establishing an electron temperature, **d** after establishing thermal equilibrium with a lattice, **e** immediately before the next LSP gets excited. **f** Evolution of the electron and lattice temperatures (not to scale as $\Delta T_e >> \Delta T_L$) through the stages (**a**–**e**). The illustrated case corresponds to the situation when the lattice cools down to the ambient temperature between the excitations

(E_F = 5.5 eV for both Au and Ag). The electron temperature rise $\Delta T_e = 2\hbar\omega E_F/\pi^2 k_B^2 T_e N_e V$ amounts to less than 4 K for a d=20 nm nanosphere and exceeds 10 K for d<15 nm and 100 K for d<7 nm (Fig. 1c). During this time period, the lattice temperature remains practically unchanged.

(d) Following that, at time $t_4 \sim t_2 + \tau_{EL}$, all the energy is transferred to the lattice, whose specific heat $c_L = 3k_B$ for gold is about 130 times higher than the specific heat of the electron gas, c_e, which leads to a very insignificant increase $\Delta T_L \sim 0.03$ K over the average lattice temperature, $\overline{T}_L$, which in turn can be found as $\overline{T}_L = T_0 + \Delta T_L f_{LSP}\tau_{LA}$, where τ_{LA} is the lattice cooling (i.e., lattice to ambient environment heat transfer) time, which is determined by the environment in which a nanoparticle is placed and can be as long as milliseconds; so that $\overline{T}_L - T_0$ may approach 100 K and more. Such a strong lattice temperature increase will definitely contribute to the hot-carrier injection from metal into adjacent dielectric or semiconductor or to chemical processes on a metal surface [29–32].

(e) By the time $t_4 \sim t_0 + f_{LSP}^{-1}$, i.e. just before the LSP is excited again both electron and lattice are once again at equilibrium with temperature $\overline{T}_L$ and the process repeats.

In the considered case of CW excitation, the increase of an instant electron temperature ΔT_e does not depend on the incoming power density I_{in} and is only a function of the nanoparticle volume. Increasing input power will only lead to the increase of the frequency with which the LSP is excited on a given nanoparticle (or, equivalently to the number of excited nanoparticles at any given time) but the electron temperature rise will remain the same. This, as well a simple fact that the lattice temperature of the nanoparticle is time dependent even though the illumination is CW, provide clear evidence of the discrete, quantum nature of the processes that take place. If one disregards the quantum nature of light absorption, then under CW illumination, one simply obtains the average steady state rise of the electron temperature $\Delta\overline{T}_e = D\Delta T_e$ with the duty cycle $D = f_{LSP}\tau_{EL}$, so that, for $\tau_{EL} \sim 200$ fs, a much smaller temperature rise $\Delta\overline{T}_e \sim 0.001\Delta T_e$ can be predicted (Fig. 1c). In this case, even for very high input powers, the average rise of electron temperature would be negligibly small [29, 30, 33].

To see the impact of this quantisation, let us consider thermionic emission of the electrons from a plasmonic nanoparticle to surroundings across the barrier Φ. In the absence of light, the emission rate is $R_{th,0} \sim \exp(-\Phi/k\overline{T}_L)$. The relative increase of the rate due to average rise of electron temperature

$$\Delta R_{th}\left(\Delta\overline{T}_e\right)/R_{th,0} \approx \exp\left(\Phi\Delta\overline{T}_e/k_B\overline{T}_L^2\right) - 1 \qquad (1)$$

is negligibly small for the achievable tiny $\Delta\overline{T}_e$ shown in Fig. 1c. On the other hand, if one properly follows the discrete nature of hot-carrier generation, one should use $\Delta T_e = \Delta\overline{T}_e/D$ in place of $\Delta\overline{T}_e$ and multiply the rate by the duty cycle D, which gives

$$\Delta\overline{R}_{th}(\Delta T_e)/R_{th,0} \approx D\left[\exp\left(\Phi\Delta\overline{T}_e/k_B D\overline{T}_L^2\right) - 1\right]. \qquad (2)$$

For $I_{in} = 100$ W cm^{-2}, $\Delta\overline{T}_e = 2\times10^{-3}$ K and for a 20 nm nanoparticle with $D = 10^{-3}$, one obtains almost the same emission rate $\Delta\overline{R}_{th}(\Delta T_e)/\Delta R_{th}\left(\Delta\overline{T}_e\right) \approx 1.05$. At the same time for a 5 nm nanoparticle with $D = 2\times10^{-5}$, it is significantly different $\Delta\overline{R}_{th}(\Delta T_e)/\Delta R_{th}\left(\Delta\overline{T}_e\right) \approx 30$. Nevertheless, the absolute value of the increase is still only $\Delta\overline{R}_{th}(\Delta T_e)/R_{th,0} \approx 0.003$.

This quantum character of absorption is preserved not just for LSPs on nanoparticles but also for SPPs propagating on a metal interface, important, for example, for the absorption in photodetectors employing metal/semiconductor interfaces. For a waveguide of length L in which the SPPs with an average power $\overline{P}$ propagate with a group velocity v_g, an average number of the SPP quanta present at any given time is $N_{SPP} = \overline{P}L/v_g\hbar\omega$. For $\overline{P}$ = 1 μW and L = 10 μM, this amounts to less than one SPP.

1.1.1 What happens under femtosecond excitation?

The situation is radically different in the case when the excitation pulse duration is comparable to the hot-electron relaxation times, i.e. under femtosecond excitation. If one considers 100 fs pulses with 80 MHz repetition rate and an average power of 1 W focused in a 100 μm spot, the peak intensities of $I_{in} \sim 10^9$ W cm^{-2} are readily achievable and hundreds of LSPs can be simultaneously excited on a single nanoparticle. Since pulse length is shorter than τ_{EL}, the entire energy of the absorbed pulse gets accumulated in the energy of hot carriers, hence the rise of electron temperature is hundreds or even thousand times larger than one caused by absorption of a single quantum of energy. The rise of the electron temperature is obviously proportional to the excitation power, and the electron temperatures of a few thousands K are not unreasonable, which may have significant influence on hot-electron photochemical processes. Remarkably, the dynamics of hot carriers and their temperature evolution for femtosecond excitation would look

very similar to Fig. 2f with magnitude of ΔT_e and ΔT_L scaled up by a number of LSPs excited, and the interval between temperature rises being regular and equal to the pulse repetition rate, rather than random. This situation is regularly encountered in nonlinear optical studies. At the same time, the maximum energy of the non-equilibrium hot carriers remains the same as determined by the energy of the single absorbed photon until multiphoton excitation processes become important at even higher excitation powers.

1.1.2 Experimental studies of hot carrier dynamics

The femtosecond excitation offers an advantage to study the relaxation mechanisms of hot carriers in great detail by using short optical pulses as time gates [34]. Ultrafast photoemission and two-photon photoemission spectroscopies have emerged as an invaluable tool for studies of the lifetime of hot carriers is metals [17, 19, 21, 22, 35], offering direct insight into hot-electron lifetimes as a function of energy. The photoemission data on traditional plasmonic metals confirm a characteristic $(E - E_F)^{-2}$ dependence of hot-electron lifetimes, as predicted by the Fermi liquid theory, save for a scaling factor that needs to be taken into account to address the additional d-band screening [22]. Time-resolved X-ray absorption spectroscopy was also used to study hot-electron dynamics in warm dense matter, including plasmonic metals [36–39]. The nonequilibrium distribution at the initial stage of evolution (Fig. 2b) can be directly visualised with the time-resolved X-ray absorption near edge structure (TR-XANES) measurements [39]. The nonlinear-optical measurements featuring ultrafast pump-probe spectroscopy are also a common tool to investigate hot-electron dynamics in plasmonic systems as will be discussed below, allowing to extract electron and phonon temperatures as well as a contribution from the non-thermalised carriers and their temporal and spatial variations.

1.1.3 Take home points

When considering the generation and decay of surface plasmons in nanoparticles or thin films, one must always consider the discrete character of all the processes taking place inside metal. The instant rise of the electron temperature may cause rise in thermionic emission, and, therefore, increased photo-injection and photocatalysis only for the smallest spherical nanoparticles under CW excitation. For large energy barriers, the absolute value of injection would still be very low. At the same time, if the lattice cooling time τ_{LA} is long (as it can be if the sample is thermally isolated from the environment), an average rise of the lattice temperature T_L may be high enough to cause a conventional thermionic emission. *Therefore, in order to achieve a carrier injection over the barrier, the non-equilibrium carriers must be present (before they thermalize to some average electron temperature), i.e. the primary electrons and holes that have not experienced a single EE scattering event.* It should be also noted that if the shape of the nanoparticle is different from the spherical or in the case of complex hereto-nanoparticles with different material components, the spatial distribution of the field enhancement is nonuniform and the hot carriers are generated nonuniformly in the nanoparticle. In this case, the mode volume (V_{eff}) is not directly related to the size of the nanoparticle and the rate of hot-electron generation is proportional to the local absorption defined by the local field, which benefits sharp edges or junctions in hetero-nanoparticles. In the case of weakly absorbing nanostructures, the rate can be enhanced by engineering dark electromagnetic states to trap the excitation light and promote absorption and hot-carrier generation. In the following sections, we describe how these carriers are generated and how they get injected from metal into semiconductors, dielectrics or molecules.

1.2 Four mechanisms of hot-carrier generation in metals

Let us now review the processes that lead to the decay of LSPs and SPPs and hot carrier generation. This issue has been widely investigated [40–52], yet some of the assumptions made in the previous works are ambiguous. In particular, it concerns the use of classical concepts to describe the LSP and SPP decay. Surface plasmons can be correctly described as collective oscillatory motion of the entire Fermi gas of the carriers with frequency ω, but its decay cannot be represented as gradual loss of energy at each half-cycle of the oscillations to some "friction force". As discussed in previous section, the surface plasmon is a quantum object with a well-defined energy $\hbar\omega$ and it can only lose this energy in an instant process in which the LSP/SPP gets annihilated and at least two new (quasi)particles are created in accordance with energy and momentum conservation laws. It is important to emphasize that "friction" loss present in the classical Drude theory is a combination of electron–electron and electron–phonon (or electron-impurity) interactions and can be adequately described by the second-order perturbation theory, widely used in condensed matter physics [24], as shown below. LSP/SPP decay in a metal is similar to phonon-assisted photon absorption in an indirect bandgap semiconductor. The quantum nature of the LSP/SPP decay is manifested in the fact that while a classic Drude "friction" rate γ behaves as T^5 at temperatures below the Debye temperature [24], at optical frequencies, the LSP/SPP decay is still very fast even at cryogenic temperatures because spontaneous emission of phonons with

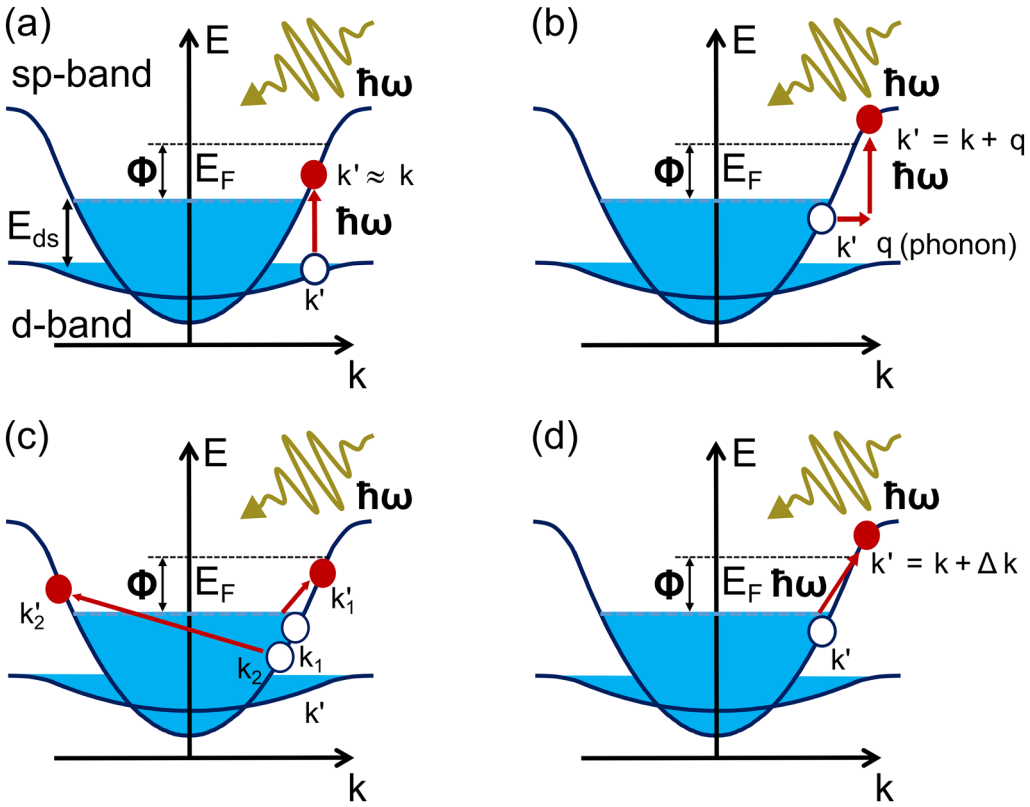

Fig. 3 Four mechanisms of electron-hole pairs generation in metals. **a** Direct (momentum conserving) interband transition exciting electron and hole with low kinetic energies. **b** Phonon (or defect/impurity) assisted indirect transition exciting electron and hole with the mean energy of each carrier $\hbar\omega/2$. **c** Transitions assisted by electron- electron scattering with two electron–hole pairs generated for each LSP/SPP with the average kinetic energies for each carrier $\hbar\omega/4$. **d** Landau damping (surface collision assisted transition), generating one electron–hole pair with an average carrier kinetic energy ħω/2. The non-equilibrium carriers produced in **b** and **d** are expected to have higher chance to overcome the surface barrier Φ and to be injected into the adjoining semiconductor or dielectric or into the adsorbed molecule

large wavevectors becomes allowed as long as a photon energy exceeds the Debye energy [53, 54].

The other issue largely overlooked in the literature is the role of the electron–electron (EE) interaction assisted processes in the LSP/SPP decay. These interactions are indeed negligibly small at low frequencies but, as frequency increases, the contribution of the EE scattering grows as $(\hbar\omega)^2$ and, at optical frequencies, the contribution of the EE scattering becomes comparable to the scattering by phonons and defects as numerous experimental results confirm [25, 55, 56].

Yet another issue concerns the holes excited in the d-bands of noble metals. While their potential energy relative to the Fermi energy may be as large as the exciting photon energy $\hbar\omega$, their kinetic energy is, however, much smaller than that, and the d-band holes excited by the interband processes usually do not reach the surface of the metal and decay after only a few nanometers. It was however demonstrated that the hot holes in the sp-band of the metal are important and may be used to drive chemical transformation in adsorbed molecules [57].

Last, but not least important misconception is that the LSP/SPP decay in metals is somehow different fundamentally from the photon absorption in dielectric or semiconductor. In fact, a photon in dielectric is also a polariton, formed by coupled oscillations of the electric field and collective oscillations of bound electrons in the valence band [58]. A significant fraction of the total energy is contained in the potential energy of these bound electrons. The only difference with surface plasmons is that a large fraction of the energy is now contained in collective oscillations of free carriers (as their kinetic energy) [59]. Hence, the decay (absorption) of LSP/SPP and photons is described by the same interaction of oscillating electric fields with the single electronic states of the medium (the interaction Hamiltonian contains only electric field and the wavefunctions of initial and final single electron states). Collective electron excitations per

se do not participate directly in the interactions and simply act as the "reservoirs" where the energy is stored during the half cycle when the electric field is small. This is equivalent to the photon-matter interactions where equal amounts of energy are carried by the electric and magnetic fields, but only electric field interacts directly with the matter in most cases. The electric field of LSPs/SPPs alone determines how they decay and what carriers are excited as the result of this decay. With this understanding, we will now consider the mechanisms that cause hot-carrier excitation.

1.2.1 Direct interband absorption

First mechanism is the direct interband (ib) absorption between the inner (4d or 5d) and outer (5sp or 6sp) shells of noble metals [47] (Fig. 3a). The energy gap separating the highest level in the d-band and the Fermi level residing in the hybridized sp-band E_{ds} is close to 2 eV for Au and 3 eV for Ag. When direct absorption takes place, the kinetic energy of the electron generated in the s-band (relative to the Fermi level) is only $E_{ib} < \hbar\omega - E_{ds}$, as can be seen in the probability of the carrier energy distribution $F_{hot,ib}(E) = 1/(\hbar\omega - E_{ds})$. If one wants to consider hot carrier injection across the barrier on the order of 0.5–1 eV, only short-wavelength (blue and UV) radiation can be used for this purpose with Au or Ag and majority of metals due to their band-gap energies. The angular distribution (with respect to the metal surface) of the non-equilibrium carriers generated via the interband absorption is uniform [27].

The holes generated in a d-band have large potential energy relative to the Fermi level, but their kinetic energy is quite low and, more important, the d-band is narrow so that electron velocity in the d-band is at least an order of magnitude lower than the Fermi velocity [60], resulting in the mean free path which is less than a nm. The holes generated in the bulk of the metal decay long before they reach the interface. For this reason, the interband absorption, as it competes with other absorption mechanisms, only reduces the efficiency of hot-carrier extraction and, for hot-carrier applications in blue-UV spectral range, the logical step is to use aluminium which does not have interband absorption in that spectral range due to absence of a d-band [61].

1.2.2 Phonon or defect assisted decay

All other LSP/SPP decay mechanisms are *intraband*, i.e. they involve absorption between two states with different electron momenta (wavevectors) in the same sp-band. This momentum mismatch needs to be somehow compensated. The momentum conservation can be delivered by either a phonon or an impurity (defect) which needs to provide a wavevector **q** (Fig. 3b). As a result, when LSP/SPP is annihilated, a hot electron and a hot hole, each with an average energy of $\hbar\omega/2$ are generated. The energy distribution of the "first generation" of hot carriers is $F_{hot,ph}(E) = 1/\hbar\omega$ with $E_F < E < E_F + \hbar\omega$ for hot electrons and $E_F > E > E_F - \hbar\omega$ for hot holes. Superficially, this process is similar to the "Drude"-like absorption arising from the imaginary part of a permittivity $\varepsilon_i = \gamma\omega_p^2/\omega^3$, and the surface plasmon damping rate due to this process is $\gamma_{ph}(\omega) = \langle\tau_{ep}^{-1}(E)\rangle_E$, where the electron–phonon (or defect) scattering rate is averaged from $E_F - \hbar\omega$ to $E_F + \hbar\omega$. At the same time, in the Drude formula, the scattering rate γ is evaluated near the Fermi level, because that is where both initial and final states of scattered carriers reside when the photon energy is small. At low temperatures, phonon scattering near the Fermi level behaves as T^5 [24] and the actual Ohmic resistance at low frequencies becomes significantly lower. However, when the photon (or LSP/SPP) energy $\hbar\omega$ substantially exceeds the Debye energy $\hbar\theta_D$ (which is few tens of meV), the phonon scattering rate exhibits much weaker temperature dependence [53] and, in fact, stays within the range of $\gamma_{ph} \approx 3 \times 10^{13}$ s^{-1} for Ag, and $\gamma_{ph} \approx 10^{14}$ s^{-1} for Au [62]. It is crucial to emphasize once again that the decay of LSP/SPP is a quantum process, not a classical one. There is no concept of "classical", "resistive", or "friction" contribution to the LSP/SPP decay, where a multitude of low-energy carriers might be created instantaneously. Instead, the energy of the surface plasmon is almost entirely transferred to just two hot particles—electron and hole—with minimal dissipation to a bath of multiple carriers near the Fermi level, except for a small phonon energy.

Nevertheless, some classical analogies still hold true even in the quantum picture. As carriers are classically accelerated along the direction of the optical field, it is expected that the photoexcited hot electrons and holes would preferentially travel in that direction. Indeed, detailed calculations reveal that the normalised angular distribution of photoexcited carriers, relative to the direction of the field (often normal to the surface), is $R_{ph}(\theta) = \frac{3}{4}cos^2\theta + \frac{1}{4}$ [47]. In many plasmonic nanostructures, the electric field near the hot spots is almost perpendicular to the surface. As a result, the fraction of hot carriers that travel towards the surface is approximately twice as large compared to a uniform distribution in the case of interband and EE-assisted scattering.

1.2.3 Electron–electron scattering assisted decay

Another LPP/SPP decay mechanism, somewhat less acknowledged within plasmonic community involves the EE scattering [56, 63] (Fig. 3c). Here two electron–hole pairs are excited by a single surface plasmon which allows both

energy and momentum conservation. At low frequencies, the EE scattering contribution to the electric resistances is negligibly small, but at optical frequencies the EE scattering grows in importance. The total momentum of carriers undergoing EE scattering is conserved: $\mathbf{k}_1' + \mathbf{k}_2' = \mathbf{k}_1 + \mathbf{k}_2$, and as long as the band can be considered parabolic near the Fermi surface, the current density is $J = -(e\hbar/m)\sum_k k$, where m is the electron effective mass. Therefore, the current is conserved, and no energy is dissipated via the EE scattering at low frequencies. But at the optical frequencies, energy of a LSP/SPP is sufficiently large to initiate the Umklapp processes [24, 64] in which one of the photo-excited electrons is promoted into the adjacent Brillouin zone so that momentum conservation relation becomes $\mathbf{k}_1' + \mathbf{k}_2' = \mathbf{k}_1 + \mathbf{k}_2 + \mathbf{g}$, where $\mathbf{g}$ is the reciprocal lattice vector. The electron velocity and current can therefore change as the result of the EE scattering, and the SPP decay involving this process becomes allowed. The EE-scattering-assisted LSP damping rate is $\gamma_{ee}(\omega) = F_U(\omega)\tau_{ee}^{-1}(\omega)$ [65] with the EE scattering rate given by

$$\tau_{ee}^{-1} \approx \frac{\pi}{24}\frac{E_F}{\hbar}\left(\frac{\hbar\omega}{E_F}\right)^2. \tag{3}$$

The EE-assisted SPP decay becomes prominent at short wavelengths and in most metals for photon energies larger than 2 eV: the EE scattering rate in noble metals is $\gamma_{ee} \sim 10^{14}$ s^{-1}, i.e. at least as large as the phonon-assisted LSP/SPP damping rate [56].

For the photon energies that are less than 1 eV, the EE-assisted damping is not important. The energy distribution of the carriers excited with assistance of the EE scattering is $F_{hot,ee}(E) = 6(\hbar\omega - E)^2/(\hbar\omega)^3$, and the mean kinetic energy of carriers is only $\hbar\omega/4$. Due to involvement of reciprocal lattice vectors, the angular distribution of the generated electrons is approximately uniform. For all three "bulk" LSP/SPP decay mechanisms discussed above, the spatial distribution of non-equilibrium carrier generation simply follows the density of the surface plasmon energy $|\boldsymbol{E}(\boldsymbol{r})|^2$, where $\boldsymbol{E}(\boldsymbol{r})$ is the electric field of the LSP/SPP.

1.2.4 Landau damping or surface collision assisted decay

The fourth and most relevant LSP/SPP decay channel (Fig. 3d) is referred to either phenomenologically as surface-collision-assisted damping or, in a quantum picture, as the Landau damping (LD) [66–69]. Classically, when the electron collides with the surface (or the "wall"), the momentum is transferred from the electron to the entire metal lattice, Consequently one can introduce the surface collision rate $\gamma_{sc} \sim v_F/d$, where d is the size of nanoparticle [70]. Note that the surface here is perfectly smooth so LD should not be confused with surface scattering by a rough surface. Quantum mechanically, the absorption is the result of the spatial localization of optical field. Since the field is localized, and discontinuous at the surface, its spatial Fourier transform contains large wavevector components, including those larger than $\Delta k = \omega/v_F$, where v_F is the Fermi velocity, which for Au and Ag is about 1.4×10^8 cm s^{-1}. These wavevector components provide necessary momentum matching to allow decay of LSP/SPP without assistance from either phonons or defects. This is commonly referred to as LD [10, 71, 72] and its origin is manifested in the fact that wavevector-dependent (nonlocal) dielectric permittivity of the metal described by the Lindhard's formula [73]

$$\varepsilon(\omega,k) = \varepsilon_b + \frac{3\omega_p^2}{k^2 v_F^2}\left[1 - \frac{\omega}{2kv_F} ln\frac{\omega + kv_F}{\omega - kv_F}\right] \tag{4}$$

has the imaginary part for $|k| > \omega/v_F$. The LSP/SPP decay rate due to the LD is $\gamma_{LD} = 3v_F/8d_{eff}$, where the effective depth is defined by the volume-to-surface ratio of the LSP/SPP mode in the metal: $d_{eff} = \int\limits_{metal} \boldsymbol{E}(\boldsymbol{r})^2 dV / \int\limits_{surface} \boldsymbol{E}_\perp^2(\boldsymbol{r}) dS$, with $\boldsymbol{E}_\perp(\boldsymbol{r})$ being the normal to the surface component of the LSP/SPP electric field (hence certain light polarizations are more favoured for hot-carrier generation than others). Both phenomenological and more exact full quantum treatments provide similar results [66]. For example, for spherical nanoparticles, $\gamma_{LD} = 0.75v_F/d$, while according to the phenomenological treatment, it is v_F/d. Therefore, the smaller is the nanoparticle, the more prominent the LD contribution is and the more efficient are all the hot-carrier driven processes.

The excited through the LD hot carriers are all located near the interface within a thin layer of thickness $\Delta L = v_F/\omega$. In other words, ΔL is the distance covered by the electron over one optical oscillation period. For example, for Au under the 700 nm wavelength excitation, it is only about 3 nm, which is obviously shorter than the mean free path of electron between collisions (typically 10–20 nm). Therefore, one half (travelling towards the surface) of the carriers excited via the LD reaches the surface; way more than in the case of the other LSP damping mechanisms. The second reason for the LD prominence is that the angular distribution of the excited carriers is nonuniform: $R_{LD}(\theta) \sim 2|cos^3\theta|$. The fraction of hot carriers that impinges on the surface at normal incidence is increased by a factor of 4 compared to the uniform distribution (characteristic for interband and EE-scattering-assisted processes) and by a factor of 2 compared to the distribution of the carriers generated by phonon-assisted processes [27]. For carrier extraction, lateral momentum conservation requires the incidence angle to be less than critical angle $\theta_c = sin^{-1}(k_s/k_F)$, where k_F is the Fermi

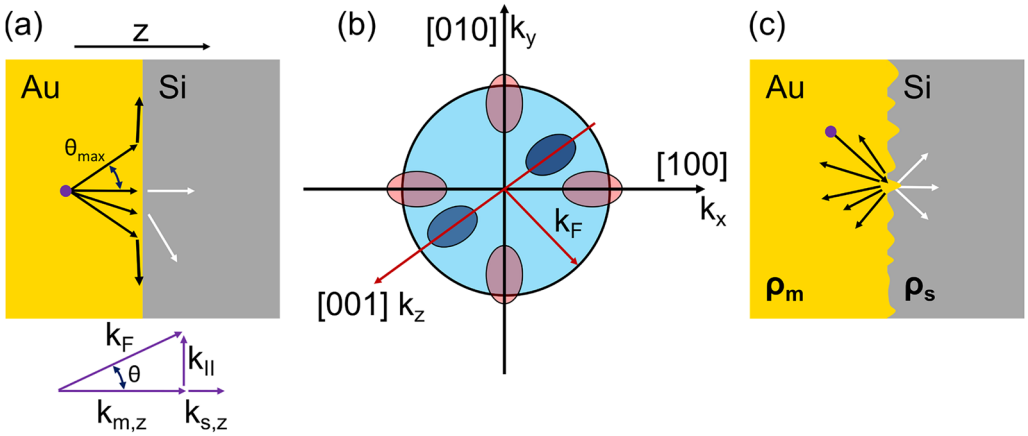

Fig. 4 Carrier injection from metal into a multi-valley semiconductor. **a** Carrier injection across a smooth interface into a multi-valley semiconductor (like Si). Injection is possible only if incidence angle less than θ_{max}. **b** Conduction band structure of Si. Electrons are injected only into the two valleys along [001] direction. **c** Carrier injection across a rough interface with lifted momentum conservation restrictions

wavevector in metal and $k_s << k_F$ is the wavevector in the adjacent medium, hence the carriers generated by the LD have the highest chance of being ejected from the metal. It should be noted that a simple treatment of the LD presented here gives results that are essentially the same as hydrodynamic theory with diffusion terms included [74–76].

2 Hot-carrier injection at a metal–semiconductor interface

An important technological application of plasmonic hot carriers lies in the field of optoelectronics and plasmonic chemistry, both requiring a charge transfer across a metal interface. At a metal–semiconductor interface, these highly energetic hot carriers may be injected from metal to semiconductor, allowing for development of improved photovoltaic devices and fast plasmonic Schottky photodetectors [77–80] and their potential efficiency is directly related to the discussion in this section.

Let us consider what happens when half of all the carriers generated near the surface by the LD as well as a (small) fraction of all the carriers generated by other mechanisms in the bulk of a plasmonic metal impinge onto the metal–semiconductor (or metal-dielectric) interface at an angle θ (Fig. 4a). The angular distribution of the impinging electrons, $R_{eff}(\theta)$, is typically determined by the LD. In the case of a smooth surface, the momentum conservation for the in-plane (lateral) electron wavevector $k_{\|} \approx k_F sin\theta$ must be maintained, as well as the energy conservation. Therefore, for the electron in the metal having the energy E above the Fermi level, the normal to the interface electron wavevector is $k_{m,z} \approx k_F cos\theta$. For a semiconductor, the wavevector component normal to the surface electron is $k_{s,z} = \sqrt{2m_L/\hbar^2(E-\Phi) - (m_L/m_T)k_{\|}^2}$, where m_L and m_T are the longitudinal and transverse effective electron masses in semiconductors, such as, for example, Si, with the band structure consisting of 6 valleys [81] (Fig. 4b). The maximum angle which still allows the propagation of the electron from metal to semiconductor is $\theta_{max}(E,\Phi) = sin^{-1}\sqrt{(m_T/m_m)(E-\Phi)/(E+E_F)}$, where m_m is the effective electron mass in the metal, typically close to the free electron mass, m_0. Using a Au/Si interface as an example, and assuming $E \sim 1$ eV, $\Phi \sim 0.5$ eV, $E_F = 5.5$ eV, and $m_T = 0.2m_0$, one obtains θ_{max}~7°, corresponding to a solid angle of $\Omega_{max} \approx 0.015\pi$, meaning that less than 1% of the incident carriers make it over the barrier. Since the incident carrier energies are typically distributed uniformly in the interval $0 < E < \hbar\omega$, the overall efficiency of the carrier injection is

$$\eta_{ext}(\hbar\omega,\Phi) = \int_0^{\hbar\omega} F_{hot}(E,\hbar\omega) \int_0^{\theta_{\max}(E,\Phi)} R_{eff}(\theta)T(\theta,E)\sin\theta d\theta dE, \tag{5}$$

where $F_{\mathrm{hot}}(E,\hbar\omega)$ depends on the type of the decay process (for simple estimations can be typically assumed $F_{hot}(E,\hbar\omega) \approx 1/\hbar\omega$) and the angle dependent electron transmission coefficient is

$$T(\theta,E) = 1 - \left(\frac{k_{m,x}/m_0 - k_{s,z}/m_L}{k_{m,z}/m_0 + k_{s,z}/m_L}\right)^2. \tag{6}$$

Note that multi-valley nature of the conduction band in indirect bandgap semiconductors, like Si or Ge, significantly affects the hot electron injection. Only two longitudinal valleys participate in the injection process since

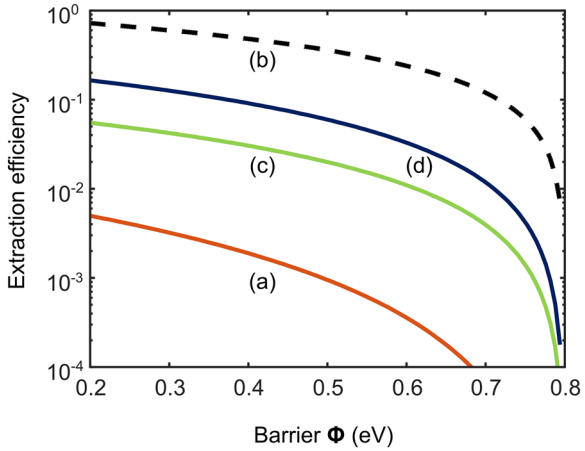

Fig. 5 The dependence of the extraction efficiency of the hot carriers at an Au/Si interface on a barrier height. **a** Smooth interface (Eq. 7), **b** rough interface with complete extraction of all the above-the-barrier carriers (Eq. 8), **c** rough interface with the momentum conservation rules relaxed but the transitions allowed only into 2 longitudinal valleys of Si (Eq. 9), and **d** rough interface with the momentum conservation rules fully lifted and the transitions into 4 transverse valleys of Si allowed (Eq. 10). The excitation wavelength is λ = 1500 nm

the $k_{\|} \sim 10^8$ cm^{-1} for the transverse valleys requires the electrons in the metal to propagate at grazing incidence to a surface where the reflection is very high.

For small values of the electron incidence angles, the approximation of Eq. 5 leads to the Fowler's formula [82]:

$$\eta_{ext}(\hbar\omega, \Phi) \approx \frac{1}{4} R_{eff}(0) T_{eff}(0) \frac{m_T}{m_0} \frac{(\hbar\omega - \Phi)^2}{\hbar\omega E_F}. \quad (7)$$

The results of the extraction efficiency calculations for a smooth Au/Si interface and the SPPs excited with $\hbar\omega = 0.8$ eV ($\lambda = 1500$ nm) show that it never approaches even 1% (Fig. 5). However, the experimental data reveal that significantly higher efficiencies can be achieved when the momentum conservation is no longer valid due to nanoscale structuring or disorder of the interface on a nanometer level (Fig. 4c). The injection efficiency of nearly 30% for a Au/GaAs interface was reported [83] and even higher 45% efficiencies for injection into TiO_2 from Au nanoparticles have been measured [84]. A ten-fold increase in photocurrent in the photodetectors with rough Au/Si interface [85] relative to the ones with a smooth interface [77] has been observed (although not all of this enhancement can be attributed to the interface roughness).

The above results can be explained assuming that nearly all the hot carriers with energies higher than barrier Φ can be extracted in the semiconductor [83]:

$$\eta_{ext}(\hbar\omega, \Phi) = \hbar\omega/\Phi - 1, \quad (8)$$

as plotted in Fig. 5b. This assumption, however, neglects the possibility of electron backscattering into a metal at an interface. More rigorous approach considers explicit description of the electron scattering on an interface roughness demonstrating the enhancement of extraction efficiency by a factor of a few [86]. The model is only applicable to a relatively small roughness and neglects the backscattering as well. Interestingly, atomically smooth interfaces of monocrystalline metal films may provide an extraction efficiency close to the theoretical limit because of the reduced hot-electron scattering, since it ensures the ballistic collection of the highly energetic electrons, particularly for ultrathin films where multiple electron scattering from the interfaces possible, as the electron mean-free-path depends on the electron energy [87]. Quasi-elastic electron–phonon scattering may also play role by redirecting the hot-electron momentum. This leads to the increase of the extraction efficiency even if there are no other mechanisms, such as lattice defects, grain boundaries and surface roughness scattering, to achieve momentum relaxation [87].

To estimate the electron extraction efficiency more rigorously, the theory developed for the seemingly different task of light trapping in the dielectric with roughened surface can be applied [88]. Since for a rough surface the momentum conservation is no longer valid, according to the Fermi's golden rule, the rate of scattering in a given direction depends only on the density of states (Fig. 4c). If the density of states in the metal and semiconductor are ρ_m and ρ_s, respectively, the extraction efficiency is [27]

$$\eta_{ext,\max}(\hbar\omega, \Phi) = \int_0^{\hbar\omega} F_{hot}(E, \hbar\omega) \frac{\rho_s(E)}{\rho_s(E) + \rho_m(E)} dE = \frac{1}{\hbar\omega} \int_0^{\hbar\omega} \frac{(m_{DOS}/m_0)^{3/2}(E - \Phi)^{1/2}/E_F^{1/2}}{(m_{DOS}/m_0)^{3/2}(E - \Phi)^{1/2}/E_F^{1/2} + 1} dE, \quad (9)$$

where m_{DOS} is the density-of-states effective mass of semiconductor [89]. For Si, if one assumes that the injection takes place in only 2 valleys along [001] direction (Fig. 4b), $m_{\mathrm{DOS}} = 2^{2/3}(m_L m_T^2) = 0.52 m_0$, resulting in injection efficiency shown in Fig. 5c. If, on the other hand, the spatial spectrum of roughness contains high spatial frequencies on the scale of $1/k_F \sim 1$ Å, then all 6 valleys can receive the injected hot carriers and $m_{DOS} = 6^{2/3}(m_L m_T^2) = 1.08 m_0$. For small extraction probability, one can obtain the approximation:

$$\eta_{ext}(\hbar\omega, \Phi) \approx \frac{2}{3} \left(\frac{m_{DOS}}{m_0} \right)^{3/2} \frac{(\hbar\omega - \Phi)^{3/2}}{\hbar\omega E_F^{1/2}}. \quad (10)$$

The extraction efficiency (Fig. 5d) estimated with Eq. (10) is not as high as expected from Eq. (8), yet it is higher than the extraction efficiency for a smooth surface described by Eq. (7). Assuming the barrier height of 0.5 eV, one can see that the enhancement by a factor of 20 to 60 can be possible leading to extraction efficiencies approaching 10%. A significant factor in the enhancement is the fact that the DOS mass is significantly larger than the transverse mass in Si, but even for semiconductors with relatively large isotropic electron mass, such as II-VI materials, the enhancement should be significant.

It should also be noted that the LSP scattering in free-space photons may reduce the absolute external quantum efficiency, however in an ensemble of nanoparticles this effect is not pronounced because the scattered light still has a chance to be absorbed by another nanoparticle. Nevertheless, in our terminology the extraction efficiency is defined as internal quantum efficiency, relative to the absorbed photon number, which remains unchanged. Similarly, the electron scattering may result in a radiative decay of hot-electrons [108], resulting in photoluminescence and, therefore, loss of energy from a metal. This process in noble metals is extremely weak and can be neglected in context of the extraction efficiency discussion.

The key point to be taken from here is that ultimately it is the density of states that determines the injection efficiency, no matter whether interface is smooth or not. Choosing semiconductor with larger effective mass (for TiO_2 it is comparable to m_0 [90]) and metal with a relatively low Fermi energy (TiN with low density of states at the Fermi level [91] comes to mind) can be highly beneficial for injection efficiency.

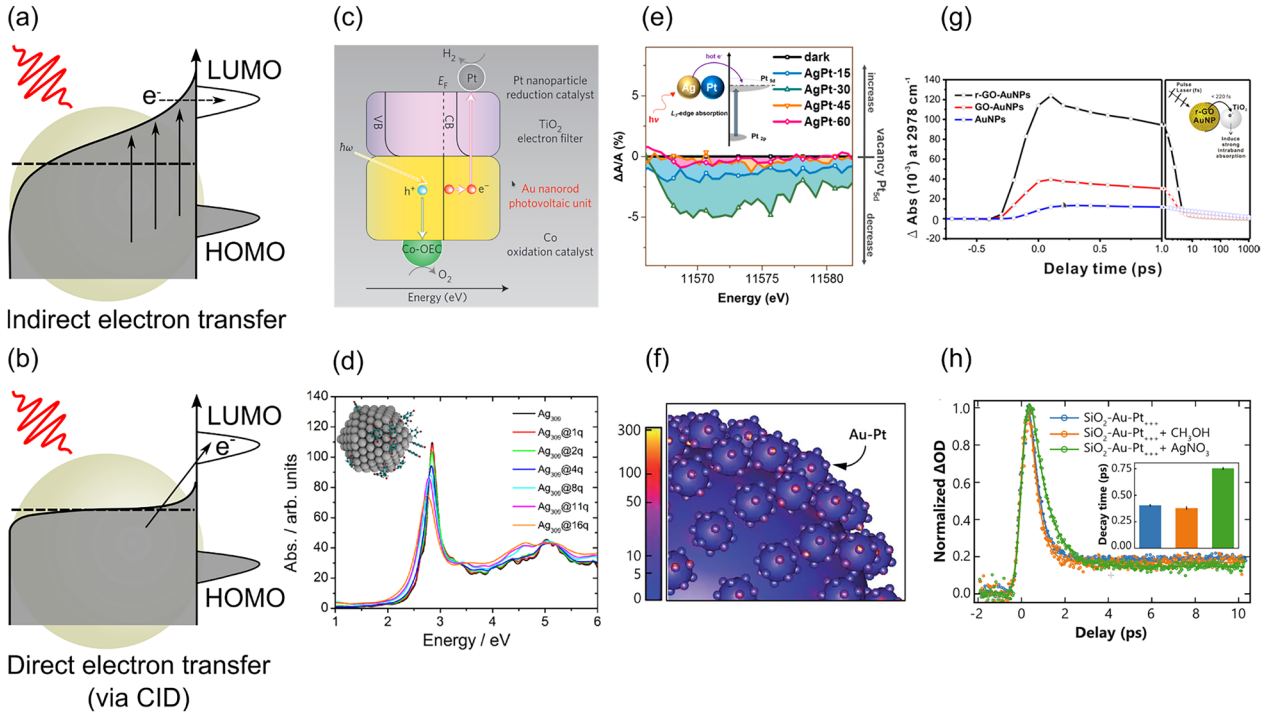

Fig. 6 Hot electrons in chemical processes. **a**, **b** Two mechanisms of hot-carrier excitations in molecular adsorbates: **a** hot-electron injection and **b** direct electron transfer (CID). **c** Design of a metal/semiconductor device for water splitting: gold nanorod is used as a source of plasmonic hot electrons, TiO_2 as a hot-electron filter, smaller Co and Pt nanoparticles act as catalysts for oxygen and hydrogen evolution [93]. **d** Atomistic calculation of broadening of plasmonic resonance of a silver cluster due to chemical interface damping (CID), induced by coupling with quinine molecules: broader peaks are obtained with higher quinine coverage [101]. **e** XANES spectra, illustrating plasmonic hot-carrier transfer in photocatalytic bimetallic Ag/Pt plasmonic alloys: optical illumination leads to a decrease in Pt_{5d} vacancy concentration affecting the reaction pathway [105]. **f** Design of plasmonic Au/Pt hetero-nanoparticles for optimized plasmocatalytic response: photocatalytic units comprised of larger plasmonic gold nanoparticles and smaller Pt nanoparticles are deposited on surfaces of large supporting silica particles [106]. **g**, **h** Transient absorption spectra for monitoring hot-carrier dynamics during chemical reactions: (**g**) Au/reduced graphene oxide (r-GO)/TiO_2 photocatalyst- transient absorption signal originating in TiO_2 from injection of plasmonic hot electrons from Au nanoparticles depends on the intermediate layer thickness [107]; (**h**) Au/Pt hetero-nanoparticles-decay of hot-carrier population in Au depends on the presence of a hot-electron scavenger $AgNO_3$ but not hot-hole scavenger CH_3OH [108]. (**c**) Reproduced with permission from [93] ©Springer-Nature 2013; (**d**) Reproduced with permission from [101] ©Amer. Chem. Soc. 2016; (**e**) Reproduced with permission from [105] ©Amer. Chem. Soc. 2017; (**d**) Reproduced with permission from [105] ©Amer. Chem. Soc. 2017; (**g**) Reproduced with permission from [107] ©Amer. Chem. Soc. 2016

3 Hot-electron chemistry

In addition to their application to photodetection, hot carriers have been recently extensively studied as a means to control chemical transformations in photochemical and photocatalytic settings [92–97]. In this context, several mechanisms need to be considered to understand the role of hot carriers and differentiate it from other processes present at the same time in the nanoplasmonic environment. These include: (i) molecular adsorption on a plasmonic material resulting in the modification of the energy levels of the molecules and, therefore, changing its reactivity, which can additionally be accompanied by the local temperature increase of the nanostructure upon illumination. The modification of the energy levels upon adsorption is a complex process, which is also influenced by the electrons in a metal near the Fermi level and, as such, not much modified by the optical excitation which changes the density of electrons near the Fermi level a little; (ii) simple increase of light-absorption by an adsorbed molecule in the vicinity of a plasmonic nanoparticle due to the field enhancement effect, which results in a conventional photochemical processes induced by light [98]; (iii) a charge (electron or hole) transfer to the adsorbed molecule; followed by (iv) product desorption. During the process (iii) in particular, a transient charged state of an adsorbate is formed with its own energy states (which are obviously different from the non-charged state) and which have different chemical reactivity. This carrier injection can occur either through the LSP/SPP decay inside a plasmonic nanostructure with subsequent injection through the interface (Fig. 6a) to the molecule (similar to the injection into a semiconductor discussed above), through hybridised surface states, or when the presence of an adsorbate on a metal surface provides additional channel of the LSP/SPP decay (similar to the defect scattering process discussed above) with the electron appearing directly in the electron accepting orbitals (LUMO) [99]. The latter process (Fig. 6b, d), sometimes referred to as 'chemical interface damping (CID) [100, 101], is favourable from the point of view of preserving the hot-carrier energy and its efficiency can be comparable to the direct electron injection [99, 102, 103].

The plasmon-induced processes allow to influence speed, efficiency, and activation barriers of chemical transformations (Fig. 6c–h), therefore there arises a possibility to manipulate selectivity and final products of the reactions. While in many cases all four contributions (i)–(iv) are important for the chemical reaction control and should all be carefully considered, the electron transfer is required in the case of oxidative/reduction (redox) reactions, and these are particularly affected by the engineered hot-electron injection. The injection of hot electrons in a surrounding solvent (even vacuum) can be achieved. During ballistic propagation in the surrounding medium, electron energy will be preserved, therefore, adsorption of molecules is not the necessary condition for inducing chemical reactions as long as the ejected electron will interact with a reactant before losing its energy. This can be used for reaction involving surrounding medium itself, such as, for example, water splitting or reactive oxygen species generation [104]. In most cases, however, the adsorption facilitates significantly the interaction between hot-electrons and reactant molecules. The adsorption of a reactant and desorption of the reaction product, needed to free site for the next cycle of the reaction, themselves depend on the local heating induced by plasmonic excitation and molecular hybridisation with a nanostructure.

An ideal plasmonic catalyst design should consider several key features: (A) efficient light absorption in a plasmonic material, which can be easily achieved near a plasmonic resonance; (B) efficient generation of hot carriers, preferably through Landau damping as discussed earlier; (C) a clear pathway for hot carriers to leave the plasmonic metal and interact with adsorbed species on a surface; and (D) a surface with appropriate surface energy for efficient adsorption. Conditions A-C can be optimized for a desired illumination wavelength by carefully choosing a plasmonic metal, as well as controlling the size and topology of the nanoparticles. However, condition D poses challenges as plasmonic metals with electronic d-bands far from the Fermi level, where adsorbate bonding and anti-bonding states are fully occupied, are unlikely to promote metal-adsorbate interactions. On the other hand, catalytic metals typically have d-bands close to the Fermi energy, promoting effective adsorption but are poor plasmonic metals in the visible and near-infrared spectral ranges. Hence, a combination of plasmonic and catalytic nanoparticles in a hetero-nanoparticle configuration (Fig. 6e, f) may be necessary to fulfil all conditions A-D. Furthermore, such a combination could potentially enhance condition B by creating additional electromagnetic field enhancements near the nanoparticle junctions, where hot carriers are generated more efficiently (either in plasmonic or directly in catalytic metal). Small catalytic nanoparticles (few nm in size) on the surface of larger plasmonic nanoparticles (few tens of nm) can also provide favourable conditions for effective hot carrier extraction by supplying additional momentum to hot electrons. This way, plasmonically-derived hot carriers are most efficiently generated and extracted at the locations where adsorbates are positioned. Semiconductor materials, typically TiO_2, have also been exploited in combination with plasmonic metals (Fig. 6c) to operate as hot electron filters separating oxidation and reductions sites [93]. It should be noted,

however, that semiconductor materials may also be detrimental to photocatalytic performance due to possibility to trap excited hot carriers. Bimetallic nanostructures (Fig. 6e, f) that do not possess interfacial Schottky barriers the hot carriers have to tunnel through, may on the other hand allow more free carriers to be available for the catalytic process. Other considerations for photocatalytic efficiency include providing a large surface area and using nanoparticles instead of planar surfaces. Several experimental bimetallic nanoreactors have been demonstrated including the gold-palladium [109], gold-rhodium [161] and aluminium-palladium [110, 111] heterostructures for hydrogen production, and gold-platinum hetero-nanoparticles [104, 106] for methylene blue photodegradation.

Understanding of hot-electron photocatalytic systems can be greatly improved with the use of conventional transient absorption spectroscopy (Fig. 6g, h). In the devices employing semiconductor materials as hot-carrier filters, it allows to study the efficacy of hot carrier transport through semiconductor [107], while in bimetallic composites the modification of electron–phonon relaxation rates could be visualised [108, 164], providing insight into hot-carrier relaxation.

The figure of merit for hot-electron-induced photocatalysis (FOM_{PC}) can be introduced considering various processes involved in the promoting chemical reaction. Experimentally, however, care should be taken comparing different performances, which may be limited by other factors, such as reactant diffusion and adsorption and product desorption rates, as well as influenced by local temperature increase due to light absorption in plasmonic nanoparticles. Taking into account the hot-electron injection rate, which depends on the light absorption rate (γ_{abs}) in plasmonic nanoparticles, the efficiency of hot carrier generation (η_{hc}) dependent on the illumination wavelength via the LSP resonant conditions, and the efficiency of hot-electron transfer to the adsorbate (η_{extr}), the FOM_{PC} of a plasmocatalyst can be expressed as $FOM_{PC} \sim \gamma_{abs}\eta_{hc}\eta_{extr}$. In turn, the light absorption rate is determined by the rate of incident photons from the illuminating light dependent on its peak intensity (I_{in}) and the absorption cross-section of the nanoparticle (σ_{abs}). Therefore, for the given conditions, the photocatalytic efficiency of the nanoparticles can be optimised by maximising the expression $FOM_{PC} \sim I_{in}\ \sigma_{abs}\eta_{hc}\eta_{extr}(r_0)$, where r_0 indicates that a hot carrier is extracted at the location of an adsorbed molecule. Generally, for the optimal designs, the presence of catalytic nanoparticles (few nm size) on a surface of plasmonic nanoparticles (20–50 nm) barely influence the absorption which is dominated by a plasmonic resonance. At the same time these plasmonic sizes are advantageous for optimising the LD generation of hot-carriers, while nanometric catalytic metal facilitate extraction from gold to catalyst-molecular hybrids. This also clearly shows the advantage of pulsed illumination as opposed to CW illumination, with the pulse duration preferably shorter than LSP decay. For complex shapes of plasmonic nanostructures, such as nanoshells, nanorods, nanopiramids, nanostars or bow-tie type antennas, the dependence of the LSP resonance position, illumination polarisation (if any) are also important since the hot-carrier generation is most efficient at the field-enhancement hot-spots and indeed the distance to the surface where extraction take place can be controlled.

4 Hot-electrons and nonlinear optical effects

Even a single LSP excitation results in the modification of the electron distribution and associated changes of the metal permittivity and refractive index. Under strong femtosecond photoexcitation, as outlined above, multiple LSP excitations may be achieved, eventually leading to a highly nonequilibrium hot-electron population in the conduction band of a metal. This hot-carrier population, inherently nonequilibrium for the first few hundred of femtoseconds (as outlined in the previous sections), subsequently decays at picosecond timescale through emission of phonons, and can be experimentally monitored using time-resolved pump-probe spectroscopy [35, 112–116].

The optical nonlinearity arises in this context from a strong dependence of the permittivity of the metal on the distribution (for non-thermalised hot carriers) or temperature (after thermalisation) of hot carriers. Indeed, the dependence of the permittivity on the intensity of light produces effective cubic Kerr-type nonlinearity, which provides opportunities to employ nanoplasmonic systems as optical switches for intensity, phase or polarisation. The permittivity of most metals is most sensitive to the excitation of hot carriers in the visible range, close to the threshold of direct interband transitions from the d-band to the vicinity of the Fermi level (e.g., around 2.35 eV for gold). Experimentally, the related "smearing" of the Fermi distribution produces a photobleaching signal above the threshold due to band filling and photoinduced absorption below the threshold [113, 117]. This spectral region is also most sensitive to the nonequilibrium hot-electron dynamics as the interband absorption makes it possible to directly probe the dynamics of occupation numbers around the Fermi level [114, 118–120]. Theoretically, this can be treated in a straightforward way employing the Fermi's golden rule for direct interband transitions [42, 121] or a full density functional approach. The variation of a permittivity of prototypical plasmonic metal (gold) under strong excitation is shown in Fig. 7d.

In the near-infrared, on the other hand, the excitation of hot carriers within the conduction band (intraband

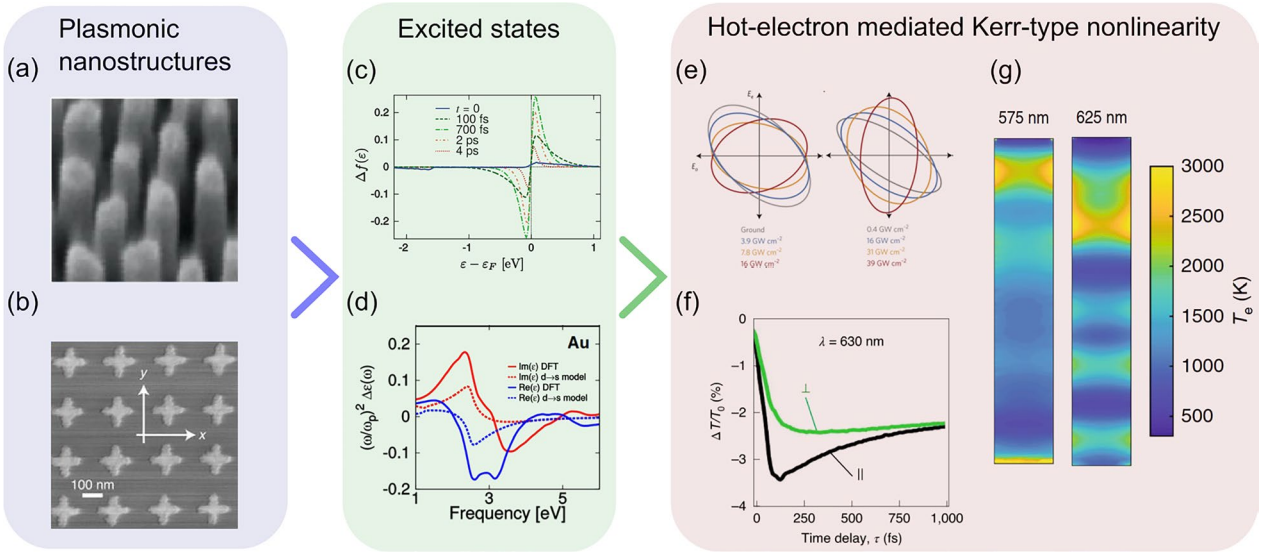

Fig. 7 From plasmonic metasurfaces to ultrafast nonlinearity. **a**, **b** Plasmonic metamaterials and metasurfaces for active control of light: **a** nanorods [122, 128] and **b** nanocrosses [129]. **c** Distributions of hot-electron energies near the Fermi level calculated from the first principles at different times after photoexcitation of a gold nanoparticle [120]. **d** Changes of the real and imaginary parts of the permittivity of gold calculated using different models, induced by an electron temperature of 5000 K [121]. **e** Optical control of polarization of light using hot-electron-induced nonlinearity in a nanorod metamaterial near the ENZ wavelength [122]: (left) pump-induced and (right) self-induced polarisation changes for different excitation powers. **f** Induced anisotropy in plasmonic nanocrosses, observed through differential transmission for aligned (black) and crossed (green) polarisations of control and probe beams [129]. **g** Local, wavelength-dependent hot-electron distributions inside gold nanorods in the metamaterial, which determine dynamics of optical response [128]. (**a**, **e**) Reproduced with permission from [122] ©Springer-Nature 2017; (**b**) Reproduced with permission from [129] ©Springer-Nature 2020; (**c**) Reproduced with permission from [120] ©Amer. Phys. Soc. 2017; (**d**) Reproduced with permission from [121] ©Amer. Phys. Soc. 2016; (**f**) Reproduced with permission from [129] ©Springer-Nature 2020

excitation) mainly contributes to the increase of the bulk damping (that appears in the Drude expression of optical conductivity of metal) due to the electron temperature dependent Umklapp electron–electron scattering [25, 55]. The latter process is sensitive to the average energy of hot carriers and, therefore, insensitive to the internal thermalisation dynamics. It is also usually weaker than changes of the permittivity close to interband transition resonances and often not observed with smooth metal surfaces outside the surface plasmon excitation condition, however the local fields enhancement in plasmonic systems allows to enhance this effect [122]. Furthermore, when Fermi level in metals lies close to the boundary of the Brillouin zone, hence the conduction band is non-parabolic, energetic hot carriers have different effective mass from the equilibrium electrons. This affects the plasma frequency and, through it, the permittivity and is the main source for hot-electron driven ultrafast manipulation of epsilon-near-zero materials [123–126]. Low free-carrier concentration in prototypical ENZ materials, such as ITO, TiN, CuO, CuS and doped ZnO, allows for much faster hot-carrier relaxation due to the increased electron–electron relaxation and, therefore, higher switching speeds [123, 127, 163].

4.1 Two-temperature model

The efficiency and speed of hot-carrier-driven nonlinear nanoplasmonic devices is linked to the dynamics of the hot-carrier decay. Since the electron thermalization time, τ_E, is at least an order of magnitude smaller than hot-electron cooling rate τ_{EL}, different stages of the dynamics (Fig. 2a–e) can be separated. Strong excitation which produces dense hot-carrier population in the conduction band facilitates "collective" thermodynamic description of the evolution based on the energy exchange between hot electrons and lattice modes (phonons). If the initial thermalisation of hot carriers (process *b* in Fig. 2) is treated instantaneously, a simple phenomenological model can be developed to describe the subsequent processes known as the two-temperature model (TTM) [35, 112, 113, 121, 130–133]. Such simplification is justified in the majority of experimental situations, where timescales above 1 ps are of interest and/or the modification of a permittivity of a metal are probed away from the interband absorption resonances. This model manifests an important distinction between hot-electron nonlinearities and hot-carrier injection discussed in the previous sections. In the latter case, the nonequilibrium electrons are of paramount importance due to the presence

of a finite energy barrier which can only be overcome by high-energy nonthermal electrons. While these electrons contribute to nonlinearity immediately after the excitation [114, 120], thermalised electron dynamics is dominant at the later times. Within the scope of the TTM, only the heat exchange between electrons and lattice, described by their corresponding temperatures (T_e and T_L, respectively) is considered coupled through the effective electron–phonon coupling constant G. The model further takes into consideration the nonlinear temperature dependence of the hot-electron specific heat c_e, derived from the free-electron model, and the dependence of the lattice heat capacity $C_L \approx c_L N$ on T_L, given by the Debye theory (it is constant above the Debye temperature). However, for most noble metals and typical experimental conditions, the rise in electron temperature does not exceed $0.1T_F$ (T_F is the Fermi temperature, which is around 6.4×10^4 K for gold [81]), therefore, a simplified expression for $C_e(T_e) = c_e N_e \approx \pi^2 k_B^2 N_e T_e / 2E_F$ may be used. These physical considerations lead to the following set of equations for electron and lattice temperatures:

$$C_e(T_e)\frac{dT_e}{dt} = \nabla(D_e(T_e, T_L)\nabla T_e) + G(T_L - T_e) + S(t) \tag{11}$$

$$C_L(T_L)\frac{dT_L}{dt} = G(T_e - T_L), \tag{12}$$

where the two additional terms in Eq. (11) describe the heat diffusion due to the electron thermal conductivity D_e and the source term $S(t)$ describing the heating by a laser pulse. In most cases, the TMM is parametrized with hot-electron heat capacity and electron–phonon coupling constants, derived from the experiment or microscopic estimates of the free-electron model [132]. An approach to use the parametrisation derived from more rigorous *ab initio* calculations have been demonstrated recently [121].

The hot-electron-induced optical transients have been extensively used not only as means for studying hot-electron dynamics in metals but as a means of active control of optical Kerr-type nonlinearities in the plasmonic systems. Numerous experimental geometries have been developed for all-optical switching applications, including, among others, LSP-based systems [129], surface plasmon polaritons [134, 135], uniaxial plasmonic composites, made of nanowires [122, 128, 136], metamaterials and metasurfaces. The geometry of the nanostructures provides additional degrees of freedom for ultrafast manipulation of optical response. Geometries like nanocrosses or aligned plasmonic nanorods (Fig. 7a, b) can be used to control optical polarisation on picosecond time scales (Fig. 7e, f) due to low symmetry of the corresponding structure. More remarkably, introducing spatial degrees of freedom in optically thick nanoplasmonic composite (Fig. 7g) allows manipulation of light polarisation at even subpicosecond timescales surpassing the limits imposed by the time constants of hot-electron decay alone. Recently, plasmonic nanostructures coupled to epsilon-near-zero materials, such as indium tin oxide, aluminium zinc oxide and others, have been widely explored for efficient optical switching applications [127]. In particular, for the realisation of the time-varying response and time-varying metamaterials, the nonparabolic conduction bands in such oxide materials provide short electron relaxation times and very large nonlinear optical changes of the refractive index.

Evolution of hot-electron population in space, occurring when the dimensions of the structure exceed the penetration depth of the optical field has been also a subject of extensive research in metals and plasmonic nanostructures. In simple experimental geometries, such as metal films, "time-of-flight" experiments were used to determine the electronic thermal conductivity $D_e(T_e, T_L)$ that appears in the refinement of the TTM [137, 138] as well as to demonstrate superdiffusive hot-electron transport on distances comparable to the electron mean free path (40–50 nm) [137]. While such transport phenomena have no charge current associated with them and only cause heat dissipation (timescale for dynamic screening in a free-electron gas is $\tau_{scr} \approx \omega_p^{-1}$, and is in femtosecond range [139]), ballistic hot electrons can nonetheless carry pure spin current if the noble metal film is interfaced with the ferromagnetic metal [140, 141], interfacing nonlinear plasmonics with the field of spintronics. Hot-electron transport phenomena can be beneficial in controlling the Kerr-type nonlinearity of plasmonic composites. For example, transport across the ensemble of long gold nanorods, allows to manipulate temporal response through variable coupling between the optical modes and hot-electron spatial distribution [128] (Fig. 7g). Buried features in metallic composites can be seen through opaque layers due to modifications of transient response induced by hot-carrier transport [142].

4.2 Beyond the two-temperature model

While the two-temperature model is only capable of treating the hot-carrier decay phenomenologically, it has been extremely successful in describing various light-induced phenomena in photoexcited metals and plasmonic nanostructures owing to its remarkable simplicity. It is easy to extend the TTM to account for additional interactions. Modifications involving nonzero phonon thermal conductivity [143], temperature-dependent electron–phonon coupling [112], spatially varying material

parameters [142] and interaction with nonequilibrium hot-electron ensemble [114, 144, 145] have been successfully demonstrated. For ferromagnetic metals, the TTM model can be extended to include the third temperature attributed to the spin population [146].

While the TTM successfully describes the cooling of the thermalized hot-electron population within $\pm k_B T_e$ (Fig. 2c) around the Fermi level, it cannot account for the initial nonequilibrium stage of the hot-carrier decay in metals. This short-lived nonequilibrium electron population is extremely important as it contains the electrons/holes with large excess energies above/below the Fermi level, which, as mentioned in the previous sections, are contributing to the electron injection from a metal. The dynamics of this non-thermal hot-electron ensemble could either accounted for through a simple rate-equation extension of the TTM (sometime referred to as "three-temperature model") [114] or, more accurately, using the Boltzmann transport equation:

$$\frac{\partial f(\boldsymbol{r},\mathbf{k},t)}{\partial t}+\dot{\boldsymbol{r}}\frac{\partial f(\boldsymbol{r},\boldsymbol{k},t)}{\partial \boldsymbol{r}}+\dot{\boldsymbol{k}}\frac{\partial f(\boldsymbol{r},\boldsymbol{k},t)}{\partial \boldsymbol{k}} = \Gamma_E[f](\boldsymbol{r},\boldsymbol{k})+\Gamma_{EL}[f](\boldsymbol{r},\boldsymbol{k})+S[f](\boldsymbol{r},\boldsymbol{k},t),$$

where Γ_E and Γ_{EL} are the collision integrals for electron–electron and electron–phonon scattering, respectively, and S refers to the source term associated with the photon or plasmon absorption. The evaluation of the collision integrals is extremely computationally demanding and for practical applications the electron–phonon scattering is almost exclusively treated in a relaxation anzats [114, 147] (even though more accurate phonon collision integrals have been used [148, 149]), while electron–electron scattering is described within the scope of the Fermi liquid theory [114, 147]. More accurately, the collision integrals can be parametrised with ab-initio-derived scalar constants [120]. The latter approach produces the dynamics of an instantaneous energy distribution of hot carriers (Fig. 7c) and is useful for studies of hot-electron injection into semiconductors [150].

The Boltzmann transport approach is currently limited to metal nanoparticles and thin films where the spatial variation of the hot-electron distribution can be ignored. This approach has been successfully employed to investigate the nonequilibrium hot- carrier dynamics in various metallic thin films and particles including silver and gold [114–116], copper [151], and chromium [133], among others. It was demonstrated, that electron thermalisation time can be controlled in plasmonic metals with the excitation fluence [120], as the lifetime of the excited electrons is inversely proportional to their energy with respect to the Fermi level. Furthermore, in nanoparticles smaller than 20 nm in diameter and ultrathin films, dynamic screening in the electron spill-out region near the surface can strongly affect the hot-electron thermalisation due to changes in the effective electron density [118, 119, 152, 153, 163].

In addition to strong modification of a linear permittivity upon excitation of hot electrons, one may envision the modification of higher-order intrinsic nonlinear susceptibility of the material. While a number of studies has explored this possibility as a tool to investigate the hot-carrier dynamics [154, 155], the changes in nonlinear susceptibilities represent the next order corrections to the optical response, and are, therefore, much weaker than the effects discussed in this section. Nevertheless, they might be observable especially in the case of ENZ materials with lower concentration of free carriers [162].

5 Conclusions and outlook

Plasmonic nanostructures harness the properties of free-electron oscillations in metals and highly doped semiconductors in order to provide strong electromagnetic field confinement and enhancement near the interfaces. This enhancement in turn assists in driving the electron gas out of equilibrium and enables a number of transient optical phenomena occurring on various timescales. As we have shown above, the nonequilibrium dynamics of hot-carrier excitation and decay are determined by the quantum nature of the processes as well as material properties and driven by the coupling between electronic, phonon and structural degrees of freedom (Fig. 8a). The exploration of hot-carrier processes in plasmonic nanostructures and control over their dynamics opens up a pathway to non-equilibrium plasmonics with applications in nanophotonics, including time-varying structures and metamaterials [156] and optical signal processing, ultrafast optoelectronics, photovoltaics, and plasmonic photochemistry (Fig. 8b). While hot carries can be excited by both CW and pulsed light and their non-equilibrium energies are the same (before the onset of the multiphoton absorption), the thermalised temperatures are strikingly different in these cases which may strongly influence related chemical and physical processes.

Hot carriers can also be generated in bulk semiconductors [157], semiconductor quantum dots [158], wires and wells [159], either by photoexcitation or applied electric field which accelerates carriers [160]. In semiconductor structures, the behaviour of hot carries has its own peculiarities and is beyond the scope of this review. While similar experimental methods can be used for its studies, only highly doped semiconductors may support plasmonic excitations relevant to the notions discussed above. Similarly, in two-dimensional materials, such as graphene, the electric field can accelerate electrons to high energies, and indeed graphene plasmons can be

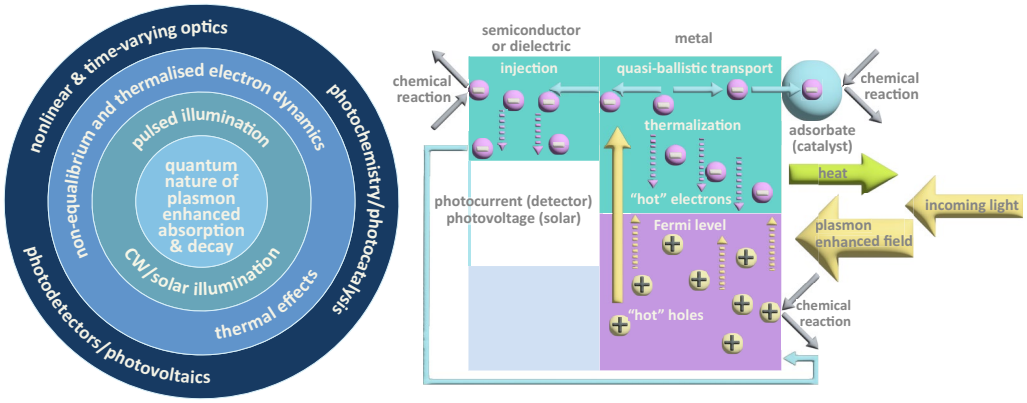

Fig. 8 Inter-relations between hot-electron processes. **a** Quantum nature of light interaction with plasmonic modes is responsible for differences in hot-carrier dynamics under CW and femtosecond pulsed illumination. Depending on the excitation regime, the generated hot-carriers result in the interconnected optical nonlinear, photochemical and/or thermal effects. **b** Schematics of hot-carrier processes in metal–semiconductor/dielectric heterostructures which interlinks photochemistry and nonlinear optics

excited in the THz spectral range, but these processes are outside the spectral range considered here for true plasmonic metals.

A persistent challenge in ultrafast plasmonic processes still evolves around enhancing the nonlinear response and control of hot-carriers dynamics. These can be addressed at both material level and exploitation of subtle properties of nanostructured media and their hybridisation with molecular or atomic species. A search for new plasmonic materials with a tailored free-carrier concentration and/or non-parabolicity of the conduction band is essential for designing the nonlinearity and engineering the carrier relaxation times. Influencing electron–electron and electron–phonon scattering rates provide an access to tailored dynamics of hot-electrons, thus offering control of the material nonlinear response time. Even for the same material, nanostructures with anisotropic electron diffusion can be used to reduce the signal switching time. Hetero-nanostructures with additional channels for electron relaxation in adjacent materials are also efficient in controlling a temporal response of nonlinearity. Similarly, an appropriately chosen environment which provides a channel for hot-carrier sink can be exploited. Ultrafast magneto-plasmonics, nano-photochemistry, ultrafast quantum optics are also important strands of applications exploiting dynamical properties of hot-carriers.

For traditional plasmonic materials, such as gold, silver and copper, the progress in fabrication and development of high quality single crystalline and ultrathin films is essential for reducing scattering losses. Single-crystalline ultrathin films approaching two-dimensional limit in thickness with atomically smooth interfaces exhibit nonequilibrium carrier dynamics different from polycrystalline films with grain boundaries, and the electron gas confinement also influences scattering processes [87]. The availability of planar plasmonic structures with ultrasmooth plasmonic surfaces would allow seamless integration with 2D materials, such as transition metal dichalcogenides and graphene. Related to the improved quality of materials and the trend toward hetero-nanostructures and molecular interactions is the requirement on improved theoretical treatment of the non-equilibrium processes which is especially important in the case of hybrid molecular-plasmonic structures, where treatment of realistic processes at the interfaces is required, including non-equilibrium electron gas, the enhanced electromagnetic field and electron transfer between molecular and plasmonic components. Other emerging topics include understanding of nonlocal effects in hot-electron generation and relaxation in the nonuniform distribution of hot carriers, including electron spill-out effects and the role of surfactants and surroundings, influencing electron density at the metal interfaces. Engineering of appropriately shaped nanoparticles and nanostructures may provide additional opportunities for harnessing increased absorption through nonradiative modes, controlling energy distribution and spatial distributions of the excited hot carriers and thus their relaxation time. Control of adsorption and desorption of molecular species mediated by the excited hot carriers is another unexplored avenue for understanding plasmonic chemistry.

Non-equilibrium plasmonics has provided numerous unique properties for designing novel applications of nanostructures, metasurfaces and metamaterials for

controlling hot-electron dynamics and the interactions of the nonequilibrium carriers with surroundings. Initially used as a means for fast reconfigurability of active functionalities employing nonlinear response, the development of our abilities to further control hot-carrier dynamics through the choice of materials, nanostructuring, and environment will further facilitate adoption of the ultrafast linear and nonlinear plasmonic devices, fast nanophotonic components, time-varying effects, nanochemistry applications and will be a basis for advancing new applications.

Acknowledgements
The authors are grateful to Megan Grace-Hughes for help with the figures.

Author contributions
J.K., A.B and A.Z. wrote and edited the manuscript.

Funding
UKRI EPSRC projects EP/W017075/1 and EP/Y015673/1.

Data availability
All the data supporting this study are presented in the article and available from the authors upon reasonable request.

Declarations

Competing interests
The authors declare no competing interests.

Received: 27 March 2024 Revised: 26 May 2024 Accepted: 4 June 2024
Published online: 16 August 2024

References

1. J. Shah, G. J. Iafrate, Hot Carriers in Semiconductors (Pergamon, 1988).
2. M.L. Brongersma, N.J. Halas, P. Nordlander, Plasmon-induced hot carrier science and technology. Nat. Nanotechnol. **10**, 25–34 (2015)
3. M. Kauranen, A.V. Zayats, Nonlinear plasmonics. Nat. Photon. **6**, 737–748 (2012)
4. P. Christopher, M. Moskovits, Hot charge carrier transmission from plasmonic nanostructures. Annu. Rev. Phys. Chem. **68**, 379–398 (2017)
5. Faraday Discussions. Vol. 214, 1–552 (Royal Soc. Chem., 2019)
6. A.V. Zayats, I.I. Smolyaninov, A.A. Maradudin, Nano-optics of surface plasmon polaritons. Phys. Rep. **408**, 131–314 (2005)
7. P. Wang et al., Molecular plasmonics with metamaterials. Chem. Rev. **122**, 15031–15081 (2022)
8. S. Lal, S.E. Clare, N.J. Halas, Nanoshell-enabled photothermal cancer therapy: impending clinical impact. Acc. Chem. Res. **41**, 1842–1851 (2008)
9. M.I. Stockman, Nanoplasmonics: past, present, and glimpse into future. Opt. Express **19**, 22029–22106 (2011)
10. J.B. Khurgin, G. Sun, R.A. Soref, Practical limits of absorption enhancement near metal nanoparticles. Appl. Phys. Lett. **94**, 071103 (2009)
11. P.B. Johnson, R.W. Christy, Optical constants of the noble metals. Phys. Rev. B **6**, 4370–4379 (1972)
12. J.B. Khurgin, U. Levy, Generating Hot carriers in plasmonic nanoparticles: when quantization does matter? ACS Photonics **7**, 547–553 (2020)
13. A.F. Koenderink, Single-photon nanoantennas. ACS Photonics **4**, 710–722 (2017)
14. K. Li, M.I. Stockman, D.J. Bergman, Self-similar chain of metal nanospheres as an efficient nanolens. Phys. Rev. Lett. **91**, 227402 (2003)
15. P. Nordlander, C. Oubre, E. Prodan, K. Li, M.I. Stockman, Plasmon hybridization in nanoparticle dimers. Nano Lett. **4**, 899–903 (2004)
16. G. Sun, J.B. Khurgin, Theory of optical emission enhancement by coupled metal nanoparticles: an analytical approach. Appl. Phys. Lett. **98**, 113116 (2011)
17. H. Petek, S. Ogawa, Femtosecond time-resolved two-photon photoemission studies of electron dynamics in metals. Prog. Surf. Sci. **56**, 239–310 (1997)
18. B. Rethfeld, A. Kaiser, M. Vicanek, G. Simon, Ultrafast dynamics of nonequilibrium electrons in metals under femtosecond laser irradiation. Phys. Rev. B **65**, 214303 (2002)
19. C.A. Schmuttenmaer et al., Femtosecond studies of carrier relaxation processes at single-crystal metal-surfaces. Proc. SPIE **2125**, 98–106 (1994)
20. A.V. Lugovskoy, I. Bray, Ultrafast electron dynamics in metals under laser irradiation. Phys. Rev. B **60**, 3279–3288 (1999)
21. W.S. Fann, R. Storz, H.W.K. Tom, J. Bokor, Electron thermalization in gold. Phys. Rev. B **46**, 13592–13595 (1992)
22. M. Bauer, A. Marienfeld, M. Aeschlimann, Hot electron lifetimes in metals probed by time-resolved two-photon photoemission. Prog. Surf. Sci. **90**, 319–376 (2015)
23. S.I. Bozhevolnyi, J.B. Khurgin, Fundamental limitations in spontaneous emission rate of single-photon sources. Optica **3**, 1418–1421 (2016)
24. J.M. Ziman, *Electrons and phonons : the theory of transport phenomena in solids* (Clarendon Press, Oxford University Press, 2001)
25. R.T. Beach, R.W. Christy, Electron-electron scattering in the intraband optical conductivity of Cu, Ag, and Au. Phys. Rev. B **16**, 5277–5284 (1977)
26. C.J. Smithells, W.F. Gale, T.C. Totemeier, *Smithells metals reference book*, 8th edn. (Elsevier Butterworth-Heinemann, Amsterdam, 2004)
27. J.B. Khurgin, Fundamental limits of hot carrier injection from metal in nanoplasmonics. Nanophotonics **9**, 453–471 (2020)
28. H. Reddy et al., Determining plasmonic hot-carrier energy distributions via single-molecule transport measurements. Science **369**, 423–426 (2020)
29. Y. Dubi, Y. Sivan, "Hot" electrons in metallic nanostructures–non-thermal carriers or heating? Light Sci. Appl. **8**, 89 (2019)
30. Y. Sivan, J. Baraban, I.W. Un, Y. Dubi, Comment on "Quantifying hot carrier and thermal contributions in plasmonic photocatalysis." Science **364**, eaaw9367 (2019)
31. Y. Sivan, Y. Dubi, Recent developments in plasmon-assisted photocatalysis–a personal perspective. Appl. Phys. Lett. **117**, 130501 (2020)
32. L. Zhou et al., Quantifying hot carrier and thermal contributions in plasmonic photocatalysis. Science **362**, 69–72 (2018)
33. Y. Sivan, I.W. Un, Y. Dubi, Assistance of metal nanoparticles in photocatalysis—nothing more than a classical heat source. Faraday Discuss. **214**, 215–233 (2019)
34. A.N. Koya et al., Advances in ultrafast plasmonics. Appl. Phys. Rev. **10**, 021318 (2023)
35. W.S. Fann, R. Storz, H.W.K. Tom, J. Bokor, Direct measurement of nonequilibrium electron-energy distributions in subpicosecond laser-heated gold films. Phys. Rev. Lett. **68**, 2834–2837 (1992)
36. P. Audebert et al., Picosecond time-resolved X-Ray absorption spectroscopy of ultrafast aluminum plasmas. Phys. Rev. Lett. **94**, 025004 (2005)
37. A. Lévy et al., X-ray absorption for the study of warm dense matter. Plasma Phys. Controlled Fusion **51**, 124021 (2009)
38. B. Mahieu et al., Probing warm dense matter using femtosecond X-ray absorption spectroscopy with a laser-produced betatron source. Nat. Commun. **9**, 3276 (2018)
39. J.-W. Lee et al., Femtosecond soft X-ray absorption spectroscopy of warm dense matter at the PAL-XFEL. J. Synchrotron Radiat. **27**, 953–958 (2020)
40. P. Narang, R. Sundararaman, H.A. Atwater, Plasmonic hot carrier dynamics in solid-state and chemical systems for energy conversion. Nanophotonics **5**, 96–111 (2016)
41. R. Sundararaman, P. Narang, A.S. Jermyn, W.A. Goddard III., H.A. Atwater, Theoretical predictions for hot-carrier generation from surface plasmon decay. Nat. Commun. **5**, 5788 (2014)
42. A.M. Brown, R. Sundararaman, P. Narang, W.A. Goddard III, H.A. Atwater, Nonradiative plasmon decay and hot carrier dynamics: effects of phonons, surfaces, and geometry. ACS Nano **10**, 957–966 (2016)

43. L.V. Besteiro, X.-T. Kong, Z. Wang, G. Hartland, A.O. Govorov, Understanding hot-electron generation and plasmon relaxation in metal nanocrystals: quantum and classical mechanisms. ACS Photonics **4**, 2759–2781 (2017)
44. A.O. Govorov, H. Zhang, Y.K. Gunko, Theory of photoinjection of hot plasmonic carriers from metal nanostructures into semiconductors and surface molecules. J. Phys. Chem. C **117**, 16616–16631 (2013)
45. G.V. Hartland, L.V. Besteiro, P. Johns, A.O. Govorov, What's so hot about electrons in metal nanoparticles? ACS Energy Lett. **2**, 1641–1653 (2017)
46. E. Blandre, D. Jalas, A.Y. Petrov, M. Eich, Limit of efficiency of generation of hot electrons in metals and their injection inside a semiconductor using a semiclassical approach. ACS Photonics **5**, 3613–3620 (2018)
47. J.B. Khurgin, Hot carriers generated by plasmons: where are they generated and where do they go from there? Faraday Discuss. **214**, 35–58 (2019)
48. A. Manjavacas, J.G. Liu, V. Kulkarni, P. Nordlander, Plasmon-induced hot carriers in metallic nanoparticles. ACS Nano **8**, 7630–7638 (2014)
49. M. Moskovits, The case for plasmon-derived hot carrier devices. Nat. Nanotechnol. **10**, 6–8 (2015)
50. I.E. Protsenko, A.V. Uskov, Photoemission from metal nanoparticles. Phys. Usp. **55**, 508 (2012)
51. L.V. Besteiro et al., The fast and the furious: Ultrafast hot electrons in plasmonic metastructures. Size and structure matter. Nano Today **27**, 120–145 (2019)
52. J.G. Liu, H. Zhang, S. Link, P. Nordlander, Relaxation of plasmon-induced hot carriers. ACS Photonics **5**, 2584–2595 (2018)
53. J.-S.G. Bouillard, W. Dickson, D.P. O'Connor, G.A. Wurtz, A.V. Zayats, Low-temperature plasmonics of metallic nanostructures. Nano Lett. **12**, 1561–1565 (2012)
54. S.V. Jayanti et al., Low-temperature enhancement of plasmonic performance in silver films. Opt. Mater. Express **5**, 1147–1155 (2015)
55. G.R. Parkins, W.E. Lawrence, R.W. Christy, Intraband optical conductivity σ(ω, T) of Cu, Ag, and Au: Contribution from electron-electron scattering. Phys. Rev. B **23**, 6408–6416 (1981)
56. M.-L. Thèye, Investigation of the optical properties of Au by means of thin semitransparent films. Phys. Rev. B **2**, 3060–3078 (1970)
57. A.E. Schlather et al., Hot hole photoelectrochemistry on Au@SiO2@Au nanoparticles. J. Phys. Chem. Lett. **8**, 2060–2067 (2017)
58. J.B. Khurgin, G. Sun, Comparative analysis of spasers, vertical-cavity surface-emitting lasers and surface-plasmon-emitting diodes. Nat. Photon. **8**, 468–473 (2014)
59. J.B. Khurgin, Relative merits of phononics vs. plasmonics: the energy balance approach. Nanophotonics **7**, 305–316 (2018)
60. T. Rangel et al., Band structure of gold from many-body perturbation theory. Phys. Rev. B **86**, 125125 (2012)
61. M.W. Knight et al., Aluminum for plasmonics. ACS Nano **8**, 834–840 (2014)
62. S. Ono, Thermalization in simple metals: Role of electron-phonon and phonon-phonon scattering. Phys. Rev. B **97**, 054310 (2018)
63. F. Abelès, *Optical properties of solids* (North-Holland Pub. Co., American Elsevier, 1972)
64. W.E. Lawrence, J.W. Wilkins, Electron-electron scattering in the transport coefficients of simple metals. Phys. Rev. B **7**, 2317–2332 (1973)
65. D. Pines, P. Nozières, The theory of quantum liquids (W.A. Benjamin, 1966)
66. J.B. Khurgin, Ultimate limit of field confinement by surface plasmon polaritons. Faraday Discuss. **178**, 109–122 (2015)
67. J. Khurgin, W.-Y. Tsai, D.P. Tsai, G. Sun, Landau damping and limit to field confinement and enhancement in plasmonic dimers. ACS Photonics **4**, 2871–2880 (2017)
68. C. Yannouleas, R.A. Broglia, Landau damping and wall dissipation in large metal clusters. Ann. Phys. **217**, 105–141 (1992)
69. Z. Yuan, S. Gao, Landau damping and lifetime oscillation of surface plasmons in metallic thin films studied in a jellium slab model. Surf. Sci. **602**, 460–464 (2008)
70. U. Kreibig, M. Vollmer, Optical properties of metal clusters (Springer, 1995)
71. T.V. Shahbazyan, Landau damping of surface plasmons in metal nanostructures. Phys. Rev. B **94**, 235431 (2016)
72. T.V. Shahbazyan, Surface-assisted carrier excitation in plasmonic nanostructures. Plasmonics **13**, 757–761 (2018)
73. J. Lindhard, On the properties of a gas of charged particles. Dan. Vid. Selsk Mat. Fys. Medd. **28**, 1–57 (1954)
74. N.A. Mortensen, S. Raza, M. Wubs, T. Søndergaard, S.I. Bozhevolnyi, A generalized non-local optical response theory for plasmonic nanostructures. Nat. Commun. **5**, 3809 (2014)
75. S. Raza, S.I. Bozhevolnyi, M. Wubs, N.A. Mortensen, Nonlocal optical response in metallic nanostructures. J. Phys. Condens. Matter **27**, 183204 (2015)
76. C. Tserkezis et al., On the origin of nonlocal damping in plasmonic monomers and dimers. Int. J. Mod. Phys. B **31**, 1740005 (2017)
77. I. Goykhman, B. Desiatov, J. Khurgin, J. Shappir, U. Levy, Waveguide based compact silicon Schottky photodetector with enhanced responsivity in the telecom spectral band. Opt. Express **20**, 28594–28602 (2012)
78. I. Goykhman, B. Desiatov, J. Khurgin, J. Shappir, U. Levy, Locally oxidized silicon surface-plasmon schottky detector for telecom regime. Nano Lett. **11**, 2219–2224 (2011)
79. I. Goykhman et al., On-chip integrated, silicon-graphene plasmonic schottky photodetector with high responsivity and avalanche photogain. Nano Lett. **16**, 3005–3013 (2016)
80. H. Lee, Y. Park, K. Song, J.Y. Park, Surface plasmon-induced hot carriers: generation, detection, and applications. Acc. Chem. Res. **55**, 3727–3737 (2022)
81. N. W. Ashcroft, N.D. Mermin, Solid State Physics (Holt-Saunders, 1976)
82. R.H. Fowler, The analysis of photoelectric sensitivity curves for clean metals at various temperatures. Phys. Rev. **38**, 45–56 (1931)
83. A. Giugni et al., Hot-electron nanoscopy using adiabatic compression of surface plasmons. Nat. Nanotechnol. **8**, 845–852 (2013)
84. D.C. Ratchford, A.D. Dunkelberger, I. Vurgaftman, J.C. Owrutsky, P.E. Pehrsson, Quantification of efficient plasmonic hot-electron injection in gold nanoparticle–TiO2 films. Nano Lett. **17**, 6047–6055 (2017)
85. S. Muehlbrandt et al., Silicon-plasmonic internal-photoemission detector for 40 Gbit/s data reception. Optica **3**, 741–747 (2016)
86. M. Grajower, U. Levy, J.B. Khurgin, The role of surface roughness in plasmonic-assisted internal photoemission schottky photodetectors. ACS Photonics **5**, 4030–4036 (2018)
87. C.O. Karaman, AYu. Bykov, F. Kiani, G. Tagliabue, A.V. Zayats, Ultrafast hot-carrier dynamics in ultrathin monocrystalline gold. Nat. Comm. **15**, 703 (2024)
88. E. Yablonovitch, Statistical ray optics. J. Opt. Soc. Am. **72**, 899–907 (1982)
89. P. Y. Yu, M. Cardona, M. Fundamentals of semiconductors: physics and materials properties (Springer, 2010)
90. C.E. Ekuma, D. Bagayoko, Ab-initio electronic and structural properties of rutile titanium dioxide. Jpn. J. Appl. Phys. **50**, 101103 (2011)
91. R. Ahuja, O. Eriksson, J.M. Wills, B. Johansson, Structural, elastic, and high-pressure properties of cubic TiC, TiN, and TiO. Phys. Rev. B **53**, 3072–3079 (1996)
92. X. Zhang, Y.L. Chen, R.-S. Liu, D.P. Tsai, Plasmonic photocatalysis. Rep. Prog. Phys. **76**, 046401 (2013)
93. S. Mubeen et al., An autonomous photosynthetic device in which all charge carriers derive from surface plasmons. Nat. Nanotechnol. **8**, 247–251 (2013)
94. Y. Zhang et al., Surface-plasmon-driven hot electron photochemistry. Chem. Rev. **118**, 2927–2954 (2018)
95. S. Linic, U. Aslam, C. Boerigter, M. Morabito, Photochemical transformations on plasmonic metal nanoparticles. Nat. Mater. **14**, 567–576 (2015)
96. E. Cortés et al., Challenges in plasmonic catalysis. ACS Nano **14**, 16202–16219 (2020)
97. M.J. Kale, T. Avanesian, P. Christopher, Direct photocatalysis by plasmonic nanostructures. ACS Catal. **4**, 116–128 (2014)
98. K. Glusac, What has light ever done for chemistry? Nat. Chem. **8**, 734–735 (2016)
99. S. Tan et al., Coherent electron transfer at the Ag/graphite heterojunction interface. Phys. Rev. Lett. **120**, 126801 (2018)
100. H. Hövel, S. Fritz, A. Hilger, U. Kreibig, M. Vollmer, Width of cluster plasmon resonances: Bulk dielectric functions and chemical interface damping. Phys. Rev. B **48**, 18178–18188 (1993)
101. O.A. Douglas-Gallardo, M. Berdakin, C.G. Sánchez, Atomistic insights into chemical interface damping of surface plasmon excitations in silver nanoclusters. J. Phys. Chem. C **120**, 24389–24399 (2016)

102. J.B. Khurgin, A. Petrov, M. Eich, A.V. Uskov, Direct plasmonic excitation of the hybridized surface states in metal nanoparticles. ACS Photon. **8**, 2041–2049 (2021)
103. D.C. Ratchford, Plasmon-induced charge transfer: challenges and outlook. ACS Nano **13**, 13610–13614 (2019)
104. J.U. Salmón-Gamboa et al., Optimizing hot carrier effects in Pt-decorated plasmonic heterostructures. Faraday Discuss. **214**, 387–397 (2019)
105. S.C. Lin, C.S. Hsu, S.Y. Chiu, T.Y. Liao, H.M. Chen, Edgeless Ag–Pt bimetallic nanocages: In situ monitor plasmon-induced suppression of hydrogen peroxide formation. J. Am. Chem. Soc. **139**, 2224–2233 (2017)
106. J.U. Salmón-Gamboa et al., Rational design of bimetallic photocatalysts based on plasmonically-derived hot carriers. Nanoscale Advances **3**, 767–780 (2021)
107. D. Kumar, A. Lee, T. Lee, M. Lim, D.-K. Lim, Ultrafast and efficient transport of hot plasmonic electrons by graphene for Pt free, highly efficient visible-light responsive photocatalyst. Nano Lett. **16**, 1760–1767 (2016)
108. A.Y. Bykov, D.J. Roth, G. Sartorello, J.U. Salmón-Gamboa, A.V. Zayats, Dynamics of hot carriers in plasmonic heterostructures. Nanophotonics **10**, 2929–2938 (2021)
109. M. Herran et al., Tailoring plasmonic bimetallic nanocatalysts toward sunlight-driven H2 production. Adv. Func. Mater. **32**, 2203418 (2022)
110. L. Yuan et al., Plasmonic photocatalysis with chemically and spatially specific antenna-dual reactor complexes. ACS Nano **16**, 17365–17375 (2022)
111. D.F. Swearer et al., Heterometallic antenna— reactor complexes for photocatalysis. Proc. Natl. Acad. Sci. **113**, 8916–8920 (2016)
112. G.L. Eesley, Generation of nonequilibrium electron and lattice temperatures in copper by picosecond laser pulses. Phys. Rev. B **33**, 2144–2151 (1986)
113. R.W. Schoenlein, W.Z. Lin, J.G. Fujimoto, G.L. Eesley, Femtosecond studies of nonequilibrium electronic processes in metals. Phys. Rev. Lett. **58**, 1680–1683 (1987)
114. C.-K. Sun, F. Vallée, L.H. Acioli, E.P. Ippen, J.G. Fujimoto, Femtosecond-tunable measurement of electron thermalization in gold. Phys. Rev. B **50**, 15337–15348 (1994)
115. N. Del Fatti et al., Nonequilibrium electron dynamics in noble metals. Phys. Rev. B **61**, 16956–16966 (2000)
116. R.H.M. Groeneveld, R. Sprik, A. Lagendijk, Femtosecond spectroscopy of electron-electron and electron-phonon energy relaxation in Ag and Au. Phys. Rev. B **51**, 11433–11445 (1995)
117. V.V. Kruglyak, R.J. Hicken, P. Matousek, M. Towrie, Spectroscopic study of optically induced ultrafast electron dynamics in gold. Phys. Rev. B **75**, 035410 (2007)
118. C. Voisin et al., Ultrafast electron-electron scattering and energy exchanges in noble-metal nanoparticles. Phys. Rev. B **69**, 195416 (2004)
119. C. Voisin et al., Size-dependent electron-electron interactions in metal nanoparticles. Phys. Rev. Lett. **85**, 2200–2203 (2000)
120. A.M. Brown et al., Experimental and ab initio ultrafast carrier dynamics in plasmonic nanoparticles. Phys. Rev. Lett. **118**, 087401 (2017)
121. A.M. Brown, R. Sundararaman, P. Narang, W.A. Goddard, H.A. Atwater, Ab initio phonon coupling and optical response of hot electrons in plasmonic metals. Phys. Rev. B **94**, 075120 (2016)
122. L.H. Nicholls et al., Ultrafast synthesis and switching of light polarization in nonlinear anisotropic metamaterials. Nat. Photon. **11**, 628–633 (2017)
123. M.Z. Alam, I. De Leon, R.W. Boyd, Large optical nonlinearity of indium tin oxide in its epsilon-near-zero region. Science **352**, 795–797 (2016)
124. J.B. Khurgin, M. Clerici, N. Kinsey, Fast and slow nonlinearities in epsilon-near-zero materials. Laser Photon. Rev. **15**, 2000291 (2021)
125. S. Sarkar, I.W. Un, Y. Sivan, Electronic and thermal response of low-electron-density drude materials to ultrafast optical illumination. Phys. Rev. Appl. **19**, 014005 (2023)
126. I.-W. Un, S. Sarkar, Y. Sivan, Electronic-based model of the optical nonlinearity of low-electron-density drude materials. Phys. Rev. Appl. **19**, 044043 (2023)
127. M.Z. Alam, S.A. Schulz, J. Upham, I. De Leon, R.W. Boyd, Large optical nonlinearity of nanoantennas coupled to an epsilon-near-zero material. Nat. Photon. **12**, 79–83 (2018)
128. L.H. Nicholls et al., Designer photonic dynamics by using non-uniform electron temperature distribution for on-demand all-optical switching times. Nat. Commun. **10**, 2967 (2019)
129. A. Schirato et al., Transient optical symmetry breaking for ultrafast broadband dichroism in plasmonic metasurfaces. Nat. Photon. **14**, 723–727 (2020)
130. S.I. Anisimov, B.L. Kapeliovich, T.L. Perel'man, Electron emission from metal surfaces exposed to ultrashort laser pulses. Sov. Phys. JETP **39**, 375–377 (1974)
131. P.B. Allen, Theory of thermal relaxation of electrons in metals. Phys. Rev. Lett. **59**, 1460–1463 (1987)
132. L. Jiang, H.-L. Tsai, Improved two-temperature model and its application in ultrashort laser heating of metal films. J. Heat Transfer **127**, 1167–1173 (2005)
133. H. Hirori, T. Tachizaki, O. Matsuda, O.B. Wright, Electron dynamics in chromium probed with 20-fs optical pulses. Phys. Rev. B **68**, 113102 (2003)
134. N. Rotenberg, J.N. Caspers, H.M. van Driel, Tunable ultrafast control of plasmonic coupling to gold films. Phys. Rev. B **80**, 245420 (2009)
135. K.F. MacDonald, Z.L. Sámson, M.I. Stockman, N.I. Zheludev, Ultrafast active plasmonics. Nat. Photon. **3**, 55–58 (2009)
136. G. Della Valle et al., Self-organized plasmonic metasurfaces for all-optical modulation. Phys. Rev. B **91**, 235440 (2015)
137. S.D. Brorson, J.G. Fujimoto, E.P. Ippen, Femtosecond electronic heat-transport dynamics in thin gold films. Phys. Rev. Lett. **59**, 1962–1965 (1987)
138. T. Juhasz, H.E. Elsayed-Ali, G.O. Smith, C. Suárez, W.E. Bron, Direct measurements of the transport of nonequilibrium electrons in gold films with different crystal structures. Phys. Rev. B **48**, 15488–15491 (1993)
139. A. Borisov, D. Sánchez-Portal, R.D.E. Muiño, P.M. Echenique, Building up the screening below the femtosecond scale. Chem. Phys. Lett. **387**, 95–100 (2004)
140. A. Melnikov et al., Ultrafast transport of laser-excited spin-polarized carriers in Au/Fe/MgO(001). Phys. Rev. Lett. **107**, 076601 (2011)
141. J. Chen et al., Competing spin transfer and dissipation at Co/Cu(001) interfaces on femtosecond timescales. Phys. Rev. Lett. **122**, 067202 (2019)
142. S. Edward et al., Detection of periodic structures through opaque metal layers by optical measurements of ultrafast electron dynamics. Opt. Express **26**, 23380–23396 (2018)
143. P. Bresson et al., Improved two-temperature modeling of ultrafast thermal and optical phenomena in continuous and nanostructured metal films. Phys. Rev. B **102**, 155127 (2020)
144. E. Carpene, Ultrafast laser irradiation of metals: beyond the two-temperature model. Phys. Rev. B **74**, 024301 (2006)
145. A. Schirato, M. Maiuri, G. Cerullo, G. Della Valle, Ultrafast hot electron dynamics in plasmonic nanostructures: experiments, modelling, design. Nanophotonics **12**, 1–28 (2023)
146. A. Kirilyuk, A.V. Kimel, T. Rasing, Ultrafast optical manipulation of magnetic order. Rev. Mod. Phys. **82**, 2731–2784 (2010)
147. G. Della Valle, M. Conforti, S. Longhi, G. Cerullo, D. Brida, Real-time optical mapping of the dynamics of nonthermal electrons in thin gold films. Phys. Rev. B **86**, 155139 (2012)
148. B.Y. Mueller, B. Rethfeld, Relaxation dynamics in laser-excited metals under nonequilibrium conditions. Phys. Rev. B **87**, 035139 (2013)
149. A. Rudenko, J.V. Moloney, Coupled kinetic Boltzmann electromagnetic approach for intense ultrashort laser excitation of plasmonic nanostructures. Phys. Rev. B **104**, 035418 (2021)
150. G. Tagliabue et al., Ultrafast hot-hole injection modifies hot-electron dynamics in Au/p-GaN heterostructures. Nat. Mater. **19**, 1312–1318 (2020)
151. X. Shen, Y.P. Timalsina, T.-M. Lu, M. Yamaguchi, Experimental study of electron-phonon coupling and electron internal thermalization in epitaxially grown ultrathin copper films. Phys. Rev. B **91**, 045129 (2015)
152. V. Halté, J. Guille, J.-C. Merle, I. Perakis, J.-Y. Bigot, Electron dynamics in silver nanoparticles: comparison between thin films and glass embedded nanoparticles. Phys. Rev. B **60**, 11738–11746 (1999)
153. C. Voisin, N. Del Fatti, D. Christofilos, F. Vallée, Ultrafast electron dynamics and optical nonlinearities in metal nanoparticles. J. Phys. Chem. B **105**, 2264–2280 (2001)
154. T.A. Luce, W. Hübner, K.H. Bennemann, Theory for the nonlinear optical response at noble-metal surfaces with nonequilibrium electrons. Z. Phys. B Condens. Matter **102**, 223–232 (1997)

155. K.L. Moore, T.D. Donnelly, Probing nonequilibrium electron distributions in gold by use of second-harmonic generation. Opt. Lett. **24**, 990–992 (1999)
156. E. Galiffi et al., Photonics of time-varying media. Adv. Photonics **4**, 014002 (2022)
157. H.M. van Driel, Kinetics of high-density plasmas generated in Si 1.06- and 0.53-um picosecond laser pulses. Phys. Rev. B **35**, 8166–8176 (1987)
158. P. Singhal, H.N. Ghosh, Hot charge carriers in quantum dots: generation, relaxation, extraction, and applications. ChemNanoMat **5**, 985–999 (2019)
159. Y. Rosenwaks et al., Hot-carrier cooling in GaAs: Quantum wells versus bulk. Phys. Rev. B **48**, 14675–14678 (1993)
160. D.K. Ferry, Hot carriers in semiconductors (IOP Publishing, 2021)
161. M.P. de Souza Rodrigues et al., Gold-rhodium nanoflowers for the plasmon-enhanced hydrogen evolution reaction under visible light. ACS Catal. **11**, 13543–13555 (2021)
162. A.Yu. Bykov, J. Deng, G. Li, A.V. Zayats, Time-dependent ultrafast quadratic nonlinearity in an epsilon-near-zero platform. Nano Lett. **24**, 3744–3749 (2024)
163. A.Yu. Bykov, A. Shukla, M. van Shilfgaarde, M.A. Green, A.V. Zayats, Ultrafast carrier and lattice dynamics in plasmonic nanocrystalline copper sulfide films. Laser Phot. Rev. **15**, 2000346 (2021)
164. M. Sachdeva, N. Ghorai, N. Kharbanda, H.N. Ghosh, Ultrafast plasmonic hot hole transfer and plasmon dynamics in a dual plasmonic Au@p-$Cu_{2-x}Se$ heterostructure. Adv. Opt. Mat. **12**, 2301250 (2024)